DETECTION OF GRAPHENE IN COVID19 VACCINES

Technical Report · November 2021

CITATIONS
0

READS
64,356

2 authors, including:

Pablo Campra
Universidad de Almería
45 PUBLICATIONS **898** CITATIONS

SEE PROFILE

DETECTION OF GRAPHENE IN COVID19 VACCINES

BY MICRO-RAMAN SPECTROSCOPY

*

TECHNICAL REPORT

Almeria, Spain, November 2, 2021

Prof. Dr. Pablo Campra Madrid
ASSOCIATE UNIVERSITY PROFESSOR
PhD in Chemical Sciences
Degree in Biological Sciences

SUMMARY

We present here our research on the presence of graphene in covid vaccines. We have carried out a random screening of graphene-like nanoparticles visible at the optical microscopy in seven random samples of vials from four different trademarks, coupling images with their spectral signatures of RAMAN vibration.

By this technique, called micro-RAMAN, we have been able to determine the presence of graphene in these samples, after **screening more than 110 objects** selected for their graphene-like appearance under optical microscopy. Out of them, a group of **28 objects have been selected, due to the compatibility of both images and spectra with the presence of graphene derivatives**, based on the correspondence of these signals with those obtained from standards and scientific literature. T**he identification of graphene oxide structures can be regarded as conclusive** in 8 of them, due to the high spectral correlation with the standard. In the remaining 20 objects, images coupled with Raman signals **show a very high level of compatibility with undetermined graphene structures**, however different than the standard used here.

This research remains open and is made available to scientific community for discussion. We make a call for independent researchers, with no conflict of interest or coaction from any institution to make wider counter-analysis of these products to achieve a more detailed knowledge of the composition and potential health risk of these experimental drugs, reminding that graphene materials have a potential toxicity on human beings and its presence has not been declared in any emergency use authorization.

DISCLAIMER

This research has been carried out exclusively by Dr. Pablo Campra, without any type of remuneration by any private or public entity, nor involvement or conformity with its results and conclusions by the institution where he is affiliated.

The characterization of the related objects corresponds exclusively to the samples analyzed. It is not possible without significant sampling to know whether these results are generalizable to other samples of similar trademarks.

Dr. Pablo Campra is only responsible for the statements written in this electronically signed file, and is not responsible for the opinions or conclusions that may be drawn from its dissemination in media and social networks and not expressed in this document, whose original version, authenticated and signed electronically, can be consulted at the following *Researchgate* platform:

https://www.researchgate.net/publication/355684360_Deteccion_de_grafeno_en_vacunas_COVID19_por_espectroscopia_Micro-RAMAN

1. ANALYTICAL METHODOLOGY

1.1. Fundamentals of the micro-Raman technique

Due to the characteristics of the sample and to the dispersion of objects with a graphene appearance of micrometric size in a complex matrix of indeterminate composition, the direct application of spectroscopic methods does not allow characterization of the nanoparticles studied here without a previous microscopic localization or fractionation from the original sample. Therefore, microscopy coupled to RAMAN spectroscopy (micro- RAMAN) was selected as an effective technique for an exhaustive screening of micrometric objects visible under the optical microscope.

RAMAN infrared spectroscopy is a fast, non-destructive technique that allows the verification of the structure of this material by identifying vibrational modes and phonons generated after excitation with monochromatic laser, generating inelastic dispersion that manifests itself in peaks of infrared emission that are a characteristic signature of the reticular structure of graphene and derivatives. Coupled optical microscopy allows the excitation laser to be focused on specific objects and points located on objects, to reinforce the degree of confidence in identifying the nature of the material, and to obtain complementary information on thickness, defects, thermal conductivity and edge geometry of graphene nanocrystalline structures.

RAMAN vibrational modes of common functional groups

O-P-O 813 cm^{-1}

C-C 800 (600-1300) cm^{-1}

C-O-C 800-970 cm^{-1} Raman average

C-(NO2) 1340-1380 cm^{-1} strong Raman; 1530-1590 cm^{-1} (asymmetrical) Medium Raman

C=C vibrations in aromatic rings (e.g. graphene, graphite)

1580-1600 cm^{-1} : Strong Raman signal

1450, 1500 cm^{-1} : Medium Raman signal

-CH2- 1465 cm^{-1} in-plane bending H-C-H (*scissoring*)

C=N 1610-1680 cm^{-1}

C=0 carbonyl 1640, 1680-1820 cm^{-1}

C-H 3000 cm^{-1}

O-H 3100-3650 cm^{-1}

1.2. Equipment used for micro-Raman spectroscopy

RAMAN LASER SPECTROMETER JASCO NRS-5100

Confocal Raman MICROSCOPE with spectrograph, includes:

-variety of magnification and working distances from x5 to x100

-up to 8 lasers ranging from UV to NIR

-SRI (spatial resolution image) to simultaneously view the sample image and the laser point.

-DSF (Dual Spatial Filtration) that optimizes the confocal focus of the image produced by the objective lens to reduce aberration and improve spatial resolution and reduce the effects of matrix fluorescence.

The spectra were analyzed with *SPECTRA MANAGER* software, version 2. JASCO Corporation.

Previously, the equipment was calibrated with a silicon standard at 520 cm^{-1}.

RAMAN spectroscopy parameters applied for screening

Data array type Linear data array
Horizontal axis Raman Shift [cm-1]
Vertical axis Int.
Start 1200 cm-1
End 1800 cm-1
Data interval 1 cm-1
Data points 601
[Measurement Information]
Model Name NRS-5100
Exposure 30 sec
Accumulation 3
Center wavenumber 1470.59 cm-1

Z position 27041.5 µm
Binning Upper 143
Binning Lower 202
Valid Channel 1 – 1024
CCD DV420_OE
Laser wavelength 532.09 nm
Monochromator Single
Grating 1800 l/mm
Wear 100 x 1000 about
Aperture d-4000 um
Notch filter 532.0 nm
Resolution 3.69 cm^{-1}, 0.96 cm^{-1}/pixel
Objective lens MPLFLN 100 x
BS/DMBS 30/70
1/2 plate Not fitted
Polarization Not fitted
Laser power 4.0 mW
Attenuator Open
CCD temperature -60.0 ºC
Shift-3.00 cm^{-1}

1.3. Micro-Raman spectroscopy of graphite and graphene

CHARACTERISTIC RAMAN BANDS OF GRAPHITE, GRAPHENE AND DERIVATIVES

- G and 2D: crystal structure of graphene and graphite

- D: crystalline mesh defects

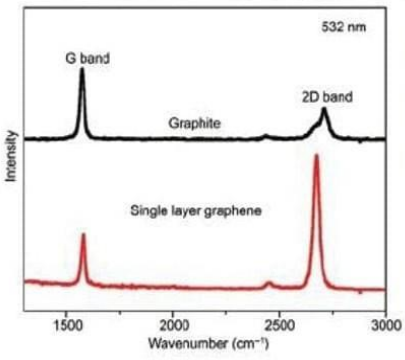

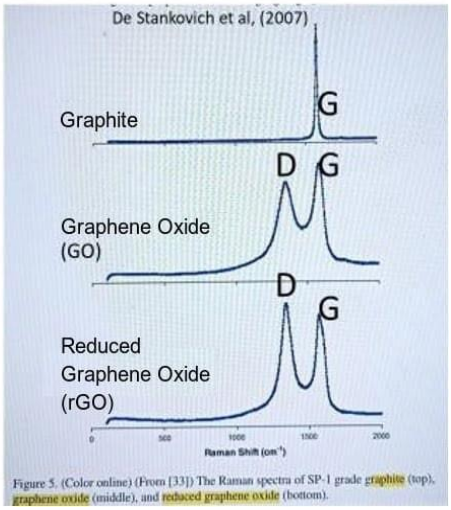

Figure 5. (Color online) (From [33]) The Raman spectra of SP-1 grade graphite (top), graphene oxide (middle), and reduced graphene oxide (bottom).

1. NANOCRYSTALLINE STRUCTURE BANDS

-**G-band (~1580-1600 cm^{-1}):** Indicates a permissible phonon vibration (elementary vibration of the net) in the plane of the aromatic ring (sp^2 hybridization), characteristic of the crystalline structure of graphite and graphene. It presents a red *shift* (lower frequency, in cm^{-1}), as well as higher intensity with a higher number of layers. On the contrary, the higher energy in doped graphene shows as a *blue shift* (higher frequency in cm^{-1}), along the 1580-1600 cm^{-1} range (Ferrari et al, 2007).

-**2D band (~2690 cm)** (or G'): Indicates stacking order. It depends on the number of layers, it does not depend on the degree of defects, but its frequency is close to twice that of peak D. Its position oscillates according to the type of doping. The presence of single-layer graphene (SLG) has been associated with the presence of an isolated and sharp 2D peak, increasing in width according to the number of layers (Ni et al., 2008).

- The ratio of I_{2D}/I_G is proportional to the number of layers of the graphite network.

- In graphite G and 2D appear are sharper and narrower than in graphene.

2. BANDS ACTIVATED BY ANOMALIES in the graphitic structure.

These bands are generated by elastic dispersion (of the same energy) of load conveyors and by phonon confinement (*Kohn's* anomaly in phonon dispersion).

In **graphene oxides (GO)** the disorder comes from the insertion of hydroxyl (-OH) and epoxide (-O-) groups.

-**D band (~1340 cm^{-1}).** It shows the density of defects in the crystal network due to functionalization, doping or structural anomalies generating holes or new sp^3 (C-C) centers. The intensity of the D-band decreases with the alignment of layers in the graphitic structure.

-**D' band (~1620 cm^{-1})**. It follows a double resonance behavior due to network defects. Sometimes it merges with the G band due to *blueshift* of the latter.

-**D+G band (~2940 cm^{-1})**

PARAMETERS INTRODUCING FREQUENCY VARIABILITY (cm^{-1}), INTENSITY AND SHAPE OF THE RAMAN BANDS

These parameters have not been studied in detail in this report but should be considered in the future for the assignment of bands to vibrational modes.

- Degree and type of **disorder** (doping, breaks, etc.), that cause wider width of the G, D, and 2D peaks by decreasing the phonon lifetime (molecular vibration)
- The G-band does not show differences in intensity due to disorder, but the ratio (I_D/I_G) does vary with D band changes.
- **Compression and stretching** of the network by **doping.** There may be *blueshifts* (>cm) in all bands (up to 15 cm^{-1} in G and 25 cm^{-1} in 2D) and band narrowing (up to 10 cm^{-1})
  e.g. "*back gates*" by doping with oxides through deposition
- By **sheet bending** the 2D band also increases, with no change in G, but with *blueshifts* between 4-12 cm^{-1} can occur.
- Stacking level or **number of layers**
- **Functionalization** (introduction of functional groups) of the network generates the appearance of new Raman peaks: 746 cm^{-1} (C–S *stretching*), 524, 1062, 1102, 1130 cm^{-1} (*skeletal vibrations*, CCCC *trans and gauche*), 1294 (*twisting*), **1440, 1461 (C–H *deformation, scissoring*),** 2848 and 2884 cm^{-1} (C–H *stretching*).
- A the same object may show spectral variations depending on the angle of incidence and the layers affected. The edges will show more disorder than the inner crystalline structure (Ni et al, 2008)
- *Blueshifts* dependent on the **substrate employed to grow** graphene layers (Chen et al, 2008)
- Variable intensity of the peaks in the same object according to the **laser focus point,** due to structural variability with respect to the angle of incidence related to the crystal network (Barros et al., 2005)

1.4. LIST OF SAMPLES OF VIALS AND OBJECTS SCREENED BY MICRO-RAMAN (SEE ANNEXES 1 AND 2)

1.5. SAMPLE PROCESSING

1. Samples were obtained from sealed vials of COVID19 mRNA vaccines as outlined in Annex 1. All vials were sealed at the time of processing, except MOD and JAN, which had no aluminum seals.

2. Four different aliquots per vial of 10 µl each were extracted with 50 µl micro-syringe, deposited on optical microscopy slides, and left to dry in aseptic laminar flow chamber at room temperature. They were then stored in a closed slide case and kept cold until micro-Raman analysis.

3. Previous extensive visual screening of drips was carried out under optical microscope (OLIMPUS CX43) in search for objects compatible with graphitic structures or graphene. Magnification from X100 to x600 were used.

Object selection criteria were:

1. Location in the remains of the droplet or in the outer area of dragging by drying
2. Two types of grafene-like appearance: two-dimensional translucent objects or dark carbon-like opaque bodies.

4. Obtain RAMAN spectra of the selected objects

5. Processing of the spectral data

The list and keys of the objects characterized in this report are set out in Annex 2.

3. RESULTS AND DISCUSSION

(See images and spectra of the selected objects in Annex 3: RESULTS)

The micro-Raman technique applied here has proved to be very effective for the rapid screening of a large number of microscopic objects in the detection of graphene micro-structures dispersed in complex samples. Compared to macro-Raman spectroscopy of whole aqueous dispersions, the combination with microscopy in micro-Raman has the advantage of allowing the association of spectral fingerprints to nanoparticles visible under the optical microscope. This technique allowed us to focus the prospection towards specific objects with graphene-like appearance, reinforcing their spectroscopic characterization with coupled images. In this work, the preliminary selection of objects has focused on two typologies, translucent sheets and opaque carbonaceous objects, due to their visual similarity with similar shapes observable in standards after sonication or in graphene oxide dispersions (see Annex 3 Results). The difference between both typologies is not due to their chemical composition, both derived from graphite, but only to the degree of exfoliation of the starting graphitic material and the number of superimposed layers, assuming a threshold of around 10 layers as a reference limit to consider that a material graphite (3D) (Ramos-Fernandez, 2017). Anyhow, it was out the scope of our work to further characterize these structures.

A total of 110 objects with graphene-like appearance were selected, mostly located at the edge of the sample droplets after dehydration, inside or outside of the dragging area by drying at room temperature of the original aqueous phase. Our of them, another 28 objects in total were selected for their higher degree of spectral compatibility with graphene materials reported in the literature, considering both spectra and images. The images and RAMAN spectra of these objects are shown in the Annex 3 of this report. It is of interest to note that the samples do not dry completely at room temperature, always leaving a gelatinous residue, whose limit can be observed in some of the photographs shown. The composition of this medium is unknown for the moment as it was not the subject of the present study, as well as that of other typologies of micrometric size objects that could be observed recurrently in the samples at low magnification (40-600X). The Raman spectra of some of these objects were obtained but are not shown in this study because they did not present visual resemblance to graphene or graphite.

A limitation in obtaining defined spectral patterns with this technique has been the intensity of the fluorescence emitted by many selected objects. In numerous translucent sheets with a graphene appearance, it was not possible to obtain Raman spectra free of fluorescence noise, so the technique did not allow to obtain specific RAMAN signals with well-defined peaks in many of them. **Therefore, in these objects the presence of graphene structures can neither be affirmed nor ruled out.** Another limitation of the micro- RAMAN technique is the low quality of the optical image of the equipment, which often prevents the detection of high-transparency graphene-like sheets, which can, however, be observed in optical microscopes with proper condenser

adjustment. For these objects an effective alternative for characterization would be to use other complementary microscopy techniques coupled with spectroscopy, such as XPS with good optics or the obtention of electron diffraction pattern of graphene by electronic microscopy (TEM).

Considering these selection criteria, the 28 objects found with potential graphene identity have been distributed in 2 groups, according to the degree of correlation with the RAMAN spectrum of reduced graphene oxide pattern used (rGO, ™SIGMA ALDRICH). **GROUP 1** included **8 objects whose spectral patterns were similar to the spectrum of the rGO pattern, and therefore** the presence **of graphene oxide (nº 1-8)** can be affirmed with certainty. This spectral correspondence can be considered **unequivocal** and is characterized by 2 dominant peaks in the scanned range (between 1200-1800 cm^{-1}), peaks called G (~1584 cm^{-1}) and D (~1344 cm^{-1}), characteristic of graphene oxides. This characterization by spectral correspondence between the signals of these nanoparticles and the rGO pattern is further reinforced by the microscopic appearance of these objects, all of them with an opaque carbonaceous appearance similar to that of the standard objects, as can be seen in the photographs in the Results annex. Therefore, **we can affirm with a high level of confidence that the identification of graphene material in all the analyzed samples of Group 1 IS CONCLUSIVE,** and with high probability graphene oxide structures can be assigned to these nanoparticles. These group 1 objects presented a micrometric size in ranges of tens of microns (shown as a blue line in photographs of some of them).

In the second group of 20 objects **(GROUP 2,** nº 9-28), **RAMAN signals compatible with the presence of graphene** or graphitic structures have been detected, showing peaks of RAMAN vibrations around the G band (1585-1600 cm^{-1}), compatible with the G peak of the nanocrystalline structure of graphene or graphite. This vibrational mode is generated by the allowed vibration of the phonon in the plane of the aromatic ring (sp^2). Its drifting towards higher frequencies in some objects, tending towards 1600 cm^{-1} *(blue shift)* can be assigned to a wide variety of modifications referred extensively in the literature, such as, for example, the number of graphene layers or doping with functional groups or heavy metals others (Ferrari et al, 2007). Visually, this group includes the two types of appearances observed in the standards: whether opaque micrometric objects with a carbonaceous appearance (nº 9, 11, 16, 21, 22, 23, 24, 25, 26, 27 and 28) or translucent sheets with graphene-like appearance (nº 10, 12, 13, 14, 18, 19 and 20).

In the spectra of this group 2, the G peak maxima are accompanied by other dominant peaks of non-determined assignment in this work. A subgroup (2.1.) can be made from of objects whose spectra have the two 2 dominant peaks located in band ranges that could be assigned to the two main vibrational modes of graphene oxide, G (range 1569-1599 cm^{-1}) and D (range 1342-1376 cm^{-1}) (objects no. 11, 14, 15, 16, 17, 20, 21, 22, 23, 24, 25 and 26). Considering both microscopic images and RAMAN signals together, the **assignation of the spectra of this group 2.1 to graphenic structures can be done with a high level of confidence. However,** although the structural modifications of the network generating spectral signals different than the standard

rGO used have yet to be determined.

The signals from a second subgroup (2.2) of objects of this Group 2 (nº 9, 10, 12, 13, 18, 19, 25, 27, 28) can be considered compatible with the presence of graphene structures due to the presence of maxima in the G-band, although the use of more detailed spectral analysis algorithms would be necessary, since no clear peaks that could be assigned to the vibrational mode D, around 1344 cm^{-1} in the rGO standard, were not clearly observed. However, the presence of peak D is not a *sine qua non* condition for the assignment of graphene structures to spectra, and in consequence these objects have been selected for this report as they are showing compatible vibrational maxima in the vicinity of the G-band (range 1569-1600 cm^{-1}). There is still an open debate about the interpretation of this D-band and its variable frequency and shape (Ferrari and Robertson, 2004). As outlined in the methodological introduction, the intensity of the D peak, generally cited around 1355 cm^{-1}, as well as the intensity ratio with the G peak (I_D / I_G) is indicative of the degree of disorder in the graphene network, introduced by different agents such as doping, introduction of very different functional groups or breaks in the continuity of the network. In ordered graphitic materials this peak D is absent. In some spectra of this subgroup 2.2., other peaks with higher frequencies *(blueshift)* than the standard appear, whose assignment to vibrational mode D is possible, although this assignment is yet to be determined by processing with algorithms analysis which was beyond the scope of the present work. Therefore, at present, for these spectra we can only state that the absence or drifting *(shift)* of the D peak with respect to the location of the rGO pattern still requires a structural interpretation according to the models available. According to the literature, both the variations in the *shift* of the G and D peaks, as well as their variable width and intensity, and the presence of other peaks seen in these spectra could be due to very diverse modifications yet to be determined, including different degrees of disorder, oxidation, doping, functionalization, and structural breaks. The study of these modifications were beyond the scope of this report.

Complementary to the range 1200-1800 $cm^{-1,}$ when RAMAN spectroscopy was extended up to 2800 cm^{-1} for some objects (nº 3, 8 and 11), a 2D peak of low intensity and frequency amplitude was detected, being absent in other scanned objects (data not shown). However, both in the rGO standard and some objects with G peak maxima, the intensity of this peak was always been very low compared to the G and D peaks of the spectra. This might be due to the fact that, in graphene oxides, the relative intensity of the 2D peak (~2700 cm^{-1}) with respect to the G and D peaks is greatly reduced. Therefore, in this study we have dispensed generally with analyzing the 2D peak for reasons of greater efficiency and use of limited resources required to scan as many objects as possible within a limited amount of time. In future work, it would be of interest to examine it for all objects, thus estimating the ratio of $I_{2D}/2_G$ intensities in those objects where it minimally manifests in this vibrational mode, which would allow for estimates to be made about the number of layers of the structure.

The objects shown in this study represent a minority portion of the total micrometric objects visible at low magnification in light-field optical microscopy (100X). These objects were scanned and are not shown in this study because their spectra where not compatible with graphene structures as they lack a band that could be assigned to G vibrational mode peak. It is of great interest to note that many of these objects show RAMAN maxima in the 1439-1457 cm^{-1} band. Likewise, among the objects in group 2.2, also a prominent peak is frequently found in this band, around 1450 cm^{-1}, in combination with peaks G and D (nº 11, 12, 14, 15, 16, 17, 20, 21, 23, 24, 25, 26 and 28). **The assignment of this band around 1450 cm^{-1} is still pending, since it does not correspond to specific peaks in graphene, but we consider it to be of great importance for the knowledge of the composition of the samples due to the frequent appearance of this vibrational mode.** As a working hypothesis, this band is usually assigned to organic methylene groups -CH_2- by bending the pair of hydrogens- (*scissoring).* However, it has also been referred to as a band of moderate intensity associated with aromatic rings, and if so, it could also be associated with graphene (Ferrari and Robertson, 2004). As stated, another possible assignment of this band would be that of a superimposed vibrational mode of some compound other than graphene, more likely, or even of the **hydrogel medium** remaining after drying, as in all samples there is always a viscous residue remaining after drying at room temperature. This residue could in many cases be manifesting RAMAN vibrations overlapping with the objects that remain embedded in it, but not in those that appear outside the gel at the limits of the drying drag zone. In this sense, it is possible that this vibrational mode of the medium appears overlapped with the G and D peaks of graphene in the spectra of subgroup 2.1. It is beyond the scope of this work to characterize this medium, as well as all the components of the sample. However, there are some substances capable of forming this hydrogel matrix whose RAMAN signals show prominent vibrational modes around this band, such as polyvinyl alcohol (PVA), methylacrylamide, or the polymer PQT-12 (Mik Andersen, https://corona2inspect.blogspot.com/ pers. com). It is also a fact that some of these substances have been combined with graphene in experimental biomedicine designs that can be found in the scientific literature, for example artificial synapses for PQT-12 (Chen and Huang, 2020), gelatins for neuronal regeneration combining methylacrylamide with graphene (Zhu et al, 2016) or PVA/GO *electrospun fibers* (Tan et al, 2016). **Now, all these hypotheses about the assignment of this peak in the vicinity of 1450 cm^{-1} remain open.**

In conclusion, out of a total of 110 scanned objects, **unambiguous signals for the presence of graphene oxide have been found in 8 objects, and signals compatible with the presence of graphitic or graphene structures in another 20 objects.** The rest of the objects scanned here, out of 110 nanoparticles with graphene-like appearance have not shown signals compatible with graphene, with spectra at times dominated by excess noise caused by excessive fluorescence intensity, so we cannot neither assign nor rule out the presence of graphene structures in them.

As a continuation of this line of work, and although our micro-RAMAN analysis has

shown conclusive signs of the presence of objects with graphene structure, to consolidate the certainty of identification and to deepen the structural characterization, it would be convenient to carry out complementary analyses using coupled microscopy and spectroscopy techniques such as XPS spectroscopy, or TEM electron diffraction.

For the present investigation, most of the samples have been obtained from sealed vials. Also, during the extraction of the samples and their transfer to slides for Raman microscopy, we worked under aseptic conditions under laminar flow chamber. However, the possibility of sample contamination processes during manufacturing, distribution, and processing, as well as the general applicability of these findings to comparable samples, need to be assessed by routine and more extensive monitoring of similar batches ofthese products.

Although the results of this sampling are conclusive with regard to **the presence of graphenic structures in some samples analyzed,** this research is considered open for continuation and is made available to the scientific community for replication and optimization, considering it necessary to continue with a more detailed and exhaustive spectral study, based on a statistically significant sampling of similar vials, and the application of complementary techniques to confirm, refute, qualify or generalize the conclusions of this report. The samples analyzed are duly guarded and available for future scientific collaboration.

CONCLUSIONS

A random sampling of COVID19 vaccine vials has been performed using a coupled micro-RAMAN technique to characterize graphene-like microscopic objects using spectroscopic fingerprints characteristic of the molecular structure.

The micro-RAMAN technique allows to reinforce the level of confidence in the identification of the material by coupling imaging and spectral analysis as observational evidence to be considered together.

Objects have been detected whose RAMAN signals by similarity with the standard unequivocally correspond to **GRAPHENE OXIDE**.

Another group of objects present variable spectral signals compatible with graphene derivatives, due to the presence of a majority of specific RAMAN signals (G-band) that can be assigned to the aromatic structure of this material, in conjunction with its visible appearance.

This research remains open for continuation, contrasting and replication. Further analyses based on significant sampling, using the described technique or others which are complementary would allow us to assess with adequate statistical significance the level of presence of graphene materials in these drugs, as well as their detailed chemical and structural characterization.

REFERENCES

Alimohammadian, M., Sohrabi, B. Observation of magnetic domains in graphene magnetized by controlling temperature, strain and magnetic field. Sci Rep 10, 21325 (2020).

Bano, I. Hussain, A.M. EL-Naggar, A.A. Albassam. Exploring the fluorescence properties of reduced graphene oxide with tunable device performance. Diamond and Related Materials, Volume 94, Pages 59-64,2019.

Barros E. B., et al, Raman spectroscopy of graphitic foams. PHYSICAL REVIEW B 71, 165422. 2005.

Biroju, Ravi, Narayanan, Tharangattu, Vineesh, Thazhe Veettil, New advances in 2D electrochemistry—Catalysis and Sensing, 2018.

Bhuyan, Sajibul Alam, Nizam Uddin, Maksudul Islam, Ferdaushi Alam Bipasha, Sayed Shafayat Hossain. Synthesis of graphene. Int Nano Lett (2016) 6:65–83

Jalil Charmi, Hamed Nosrati, Jafar Mostafavi Amjad, Ramin Mohammadkhani, Hosein Danafar. Polyethylene glycol (PEG) decorated graphene oxide nanosheets for controlled release curcumin delivery. VOLUME 5, ISSUE 4, E01466, APRIL 01, 2019

Childres, Luis A. Jaureguib,, Wonjun Parkb, Helin Caoa, and Yong P. Chena et al RAMAN SPECTROSCOPY OF GRAPHENE AND RELATED MATERIALS. [www.physics.purdue.edu]. Last Accessed 30/10/21.

Choucair, Mohammad, Thordarson, Pall, Stride, John, Gram-scale production of graphene based on solvothermal synthesis and sonication. Nature nanotechnology, 2009.

Chung, Hoon & Zelenay, Piotr. (2015). Chung and Zelenay, Chem Commun 2015 (on-line version). A Simple Synthesis of Nitrogen-Doped Carbon Micro- and Nanotubes.

Colom, J. Cañavate, M.J. Lis, G. Sanjuan, and I. Gil. Structural analysis of Graphene Oxides (GO) and Reduced Graphene Oxides (rGO). 2020

Durge, Rakhee & Kshirsagar, R.V. & Tambe, Pankaj. (2014). Effect of Sonication Energy on the Yield of Graphene Nanosheets by Liquid-phase Exfoliation of Graphite. Procedia Engineering. 97. 10.1016/j.proeng.2014.12.429.

Fakhrullin R., Läysän Nigamatzyanova, Gölnur Fakhrullina, Dark-field/hyperspectral microscopy for detecting nanoscale particles in environmental nanotoxicology research. Science of The Total Environment. Volume 772,2021.

Fan, Qitang, Martin-Jimenez, Daniel, Ebeling, Daniel, Krug, Claudio K., Brechmann, Lea, Kohlmeyer, Corinna et al. Nanoribbons with Nonalternant Topology from Fusion of Polyazulene: Carbon Allotropes beyond Graphene. Journal of the American Chemical Society. 2019

Ferrari A.C. / Raman spectroscopy of graphene and graphite: Disorder, electron–phonon coupling, doping and nonadiabatic effects. Solid State Communications 143 (2007)

Ferrari AC and J. Robertson Interpretation of Raman spectra of disordered and amorphous carbon. Phys. Rev. B **61**, 2000

Ferrari Andrea Carlo and Robertson John. Raman spectroscopy of amorphous, nanostructured, diamond–like carbon, and nanodiamond. Phil. Trans. R. Soc. A.3622477–2512. 2004

Fraga, Tiago José Marques, da Motta Sobrinho, Maurício Alves, Carvalho, Marilda Nascimento, Ghislandi, Marcos Gomes. State of the art: synthesis and characterization of functionalized graphene nanomaterials. Nano Express. 2020. IOP Publishing.

Gao, A.; Chen, S.; Zhao, S.; Zhang, G.; Cui, J.; Yan, Y. (2020). The interaction between N, N- dimethylacrylamide and pristine graphene and its role in fabricating a strong nanocomposite hydrogel. Journal of Materials Science, 55(18).

Gupta A., Gugang Chena, P. Joshi, Tadigadapa S., and P.C. Eklund. Raman Scattering from High Frequency Phonons in Supported n-Graphene Layer Films. https://arxiv.org/ftp/cond- mat/papers/0606/0606593.pdf (last accessed 31/10/21)

Gusev A, Zakharova O, Muratov DS, Vorobeva NS, Sarker M, Rybkin I, Bratashov D, Kolesnikov E, Lapanje A, Kuznetsov DV, Sinitskii A. Medium-Dependent Antibacterial Properties and Bacterial Filtration Ability of Reduced Graphene Oxide. Nanomaterials (Basel). 2019 Oct 13;9(10):1454. doi: 10.3390/nano9101454. PMID: 31614934; PMCID: PMC6835404.

Hack R, Cláudia Hack, Gumz Correia, Ricardo Antônio de Simone Zanon, Sérgio Henrique Pezzin Matéria (Rio J.) 23 (1) Characterization of graphene nanosheets obtained by a modified Hummer's method. 2018.

Hu, X., Dandan Lia and Li Mu. Biotransformation of graphene oxide nanosheets in blood plasma affects their interactions with cells. Environ. Sci.: Nano, 2017,4, 1569-1578.

Alison J. Hobro, Mansour Rouhi, Ewan W. Blanch* and Graeme L. Conn. Raman and Raman optical activity (ROA) analysis of RNA structural motifs in Domain I of the EMCV IRES. Nucleic Acids Research, 2007, Vol. 35, No. 4 1169–1177

Long-Xian Gai, Wei-Qing Wang, Xia Wu, Xiu-Jun Su, Fu-Cun Yang, NIR absorbing reduced graphene oxide for photothermal radiotherapy for treatment of esophageal cancer, Journal of Photochemistry and Photobiology B: Biology, Volume 194, 2019, Pages 188-193.

Khalilia D. Graphene oxide: a promising carbocatalyst for the regioselective thiocyanation of aromatic amines, phenols, anisols and enolizable ketones by hydrogen peroxide/KSCN in water. New J. Chem., 2016,40, 2547-2553

Khare, R., Dhanraj B. Shinde, Sanjeewani Bansode, Mahendra A. More, Mainak Majumder, Vijayamohanan K. Pillai, and Dattatray. Graphene nanoribbons as prospective field emitter. J. Appl. Phys. Lett. 106, 023111 (2015). 2015

Kim S, Lee SM, Yoon JP, Lee N, Chung J, Chung WJ, Shin DS. Robust Magnetized Graphene Oxide Platform for In Situ Peptide Synthesis and FRET-Based Protease Detection. Sensors (Basel). Sep 15;20(18):5275. 2020

Jaemyung Kim, Franklin Kim, Jiaxing Huang, Seeing graphene-based sheets, Materials Today, Volume 13, Issue 3, Pages 28-38. 2010

Kovaříček et al. Extended characterization methods for covalent functionalization of graphene on copper, Carbon, Volume 118 (2017)

Jia-Hui Liu et al. Biocompatibility of graphene oxide intravenously administrated in mice— effects of dose, size and exposure protocols. Toxicol. Res., 2015,4, 83-91.

Kozawa D, Miyauchi Y, Mouri S, Matsuda K. Exploring the Origin of Blue and Ultraviolet Fluorescence in Graphene Oxide. J Phys Chem Lett. 2013 Jun 20;4(12):2035-40. 2013.

Liao Y, Zhou X, Fu Y, Xing D. Graphene Oxide as a Bifunctional Material toward Superior RNA Protection and Extraction. ACS Appl Mater Interfaces. 2018 Sep 12;10(36):30227-30234. 2018

Lu N, Huang Y, Li HB, Li Z, Yang J. First principles nuclear magnetic resonance signatures of graphene oxide. J Chem Phys. 2010 Jul 21;133(3):034502. doi: 10.1063/1.3455715. PMID: 20649332.

Manoratne C.H., S.R.D.Rosa, and I.R.M. Kottegoda. XRD-HTA, UV Visible, FTIR and SEM Interpretation of Reduced Graphene Oxide Synthesized from High Purity Vein Graphite. Material Science Research India Vol. 14(1), 19-30 (2017).

Marquina, J.;I Power, Ch.II. and González, J. III. Raman spectroscopy of graphene monolayer and graphite: electron phonon coupling and non-adiabatic effects. Tumbaga Magazine 2010 | 5 | 183-194

Martin-Gullon, I, Juana M. Pérez, Daniel Domene, Anibal J.A. Salgado-Casanova, Ljubisa R. Radovic, New insights into oxygen surface coverage and the resulting two-component structure of graphene oxide, Carbon, Volume 158, 2020, Pages 406-417

Meyer, J., Geim, A., Katsnelson, M. et al. The structure of suspended graphene sheets. Nature 446, 60–63 (2007).

Ni, Z., Wang Y, and Shen Z. Raman Spectroscopy and Imaging of Graphene, Nano Res (2008) 1: 273 291

Palacio I, Koen Lauwaet, Luis Vázquez, Francisco Javier Palomares a, Héctor González-Herrero, José Ignacio Martínez, Lucía Aballe, Michael Foerster, Mar García-Hernández and José Ángel Martín-Gago. Ultra-thin NaCl films as protective layers for Graphene. Nanoscale, 2019, 11, 16767-16772

Palmieri V, Perini G, De Spirito M, Papi M. Graphene oxide touches blood: in vivo interactions of bio-coronated 2D materials. Nanoscale Horiz. 2019 Mar 1;4(2):273-290. doi: 10.1039/c8nh00318a. Epub 2018 Oct 31. PMID: 32254085.

Panchal V, Yang Y, Cheng G, Hu J, Kruskopf M, Liu CI, Rigosi AF, Melios C, Hight Walker AR, Newell DB, Kazakova O, Elmquist RE. Confocal laser scanning microscopy for rapid optical characterization of graphene. Commun Phys. 2018

Paredes JI, Villar-Rodil S, Martínez-Alonso A, Tascón JM. Graphene oxide dispersions in organic solvents. Langmuir. 24(19):10560-4. 2008

Ramos Fernandez Gloria. Effect of the surface chemistry of graphene oxide in the development of Applications. DOCTORAL THESIS. University of Alicante. 2017.

Sadezky, A. H. Muckenhuber, H. Grothe, R. Niessner, U. Pöschl, Raman microspectroscopy of soot and related carbonaceous materials: Spectral analysis and structural information, Carbon, Volume 43, Issue 8,2005, Pages 1731-1742

Sarkar, S.K., K.K. Raul, S.S. Pradhan, S. Basu, A. Nayak, Magnetic properties of graphite oxide and reduced graphene oxide, Physica E: Low-dimensional Systems and Nanostructures,Volume 64, 2014,Pages 78-82.

Smetana Jr.K.; Vacik, J.; Součková, D.; Krčová, Z.; Šulc, J. (1990). The influence of hydrogel functional groups on cell behavior. Journal of biomedical materials research, 24(4), pp. 463-470.

Stankovich S, Dmitriy A. Dikin, Richard D. Piner, Kevin A. Kohlhaas, Alfred Kleinhammes, Yuanyuan Jia, Yue Wu, SonBinh T. Nguyen, Rodney S. Ruoff, Synthesis of graphene-based nanosheets via chemical reduction of exfoliated graphite oxide, Carbon, Volume 45, Issue 7, 2007, Pages 1558-1565.

Thema F.T., M. J. Moloto, E. D. Dikio, N. N. Nyangiwe, L. Kotsedi, M. Maaza, M. Khenfouch, "Synthesis and Characterization of Graphene Thin Films by Chemical Reduction of Exfoliated and Intercalated Graphite Oxide", Journal of Chemistry, vol. 2013, Article ID 150536, 6 pages, 2013.

Uran S., A. Alhani, and C. Silva, Study of ultraviolet-visible light absorbance of exfoliated graphite forms, AIP Advances 7, 035323 (2017)

Wang, J.W., Hon, M.H. Preparation and characterization of pH sensitive sugar mediated (polyethylene glycol/chitosan) membrane. Journal of Materials Science: Materials in Medicine 14, 1079–1088 (2003).

Yang, S.H., Lee, T., Seo, E., Ko, E.H., Choi, I.S. and Kim, B.-S. (2012), Interfacing Living Yeast Cells with Graphene Oxide Nanosheets. Macromol. Biosci., 12: 61-66.

Ye, Y.; Hu, X. (2016). A pH-sensitive injectable nanoparticle composite hydrogel for anticancer drug delivery. Journal of Nanomaterials, 2016.

Wei Zhu, Harris BT, Zhang LG. Gelatin methacrylamide hydrogel with graphene nanoplatelets for neural cell-laden 3D bioprinting. Annu Int Conf IEEE Eng Med Biol Soc. 2016 Aug;2016:4185- 4188. doi: 10.1109/EMBC.2016.7591649. PMID: 28269205.

ANNEX 1

COVID19 mRNA vaccines subject to micro-RAMAN analysis

PFIZER 1 (RD1). Batch EY3014. Sealed

PFIZER 2 (WBR). Batch FD8271. Sealed

PFIZER 3 (ROS). Batch F69428. Sealed

PFIZER 4 (ARM). Batch FE4721. Sealed

ASTRAZENECA (AZ MIT). Batch ABW0411. Sealed

MODERN (MOD). Batch 3002183. Not sealed

JANSSEN (JAN). Batch number Not available. Not sealed

GRAPHENE STANDARD SAMPLES

Reduced graphene oxide (rGO) (™Sigma Aldrich. Ref 805424)

GRAPHENE OXIDE Suspension (™The Graphene Box)

ANNEX 2

CHARACTERIZED OBJECTS COMPATIBLE WITH GRAPHENE STRUCTURES

GROUP 1

1 PFIZER 2 WBR UP GO2
2 PFIZER 3 Ros 2hy GO1
3 PFIZER 3 Ros 2hy GO1b
4 PFIZER 3 Ros 2hy b GO2
5 AZ MIT UP CARB1
6 AZ MIT UP CARB4
7 AZ MIT DOWN CARB2
8 MOD lump1

GROUP 2

9 PFIZER 2 WBR GO1
10 PFIZER 2 WBR GO6a
11 PFIZER 2 WBR 2 GO7
12 PFIZER 2 WBR UP GO1
13 PFIZER 2 WBR UP GO3b
14 PFIZER 2 WBR UP GO4
15 PFIZER 2 WBR DOWN GO2
16 PFIZER 2 WBR DOWN GO3
17 PFIZER 2 WBR DOWN GO5
18 PFIZER 3 ROS OBJ 1
19 PFIZER 3 ROS 2 OBJ 1
20 PFIZER 3 ROS 2 OBJ 2
21 PFIZER 4 Pdown lump1
22 PFIZER 4 Pdown lump2
23 PFIZER 4 Pdown lump3
24 ASTRAZENECA AZ MIT UP CARB5
25 ASTRAZENECA AZ MIT UP CARB6
26 JANSSEN JAN GO1
27 JANSSEN JAN GO3
28 JANSSEN JAN GO4

ANNEX 3. RESULTS

Detection of graphene in COVID19 vaccines using micro-RAMAN spectroscopy

TECHNICAL REPORT

ANNEX 3. RESULTS

Almería, Spain November 2, 2021

Prof. Dr. Pablo Campra Madrid
ASSOCIATE UNIVERSITY PROFESSOR
PhD in Chemical Sciences
Degree in Biological Sciences

VIALS ANALYZED by micro-RAMAN

<u>COVID19 mRNA VACCINES</u>

PFIZER 1 (RD1). Batch # EY3014. Sealed

PFIZER 2 (WBR). Batch # FD8271. sealed

PFIZER 3 (ROS). Batch # F69428. Sealed

PFIZER 4 (ARM). Batch # FE4721. Sealed

ASTRAZENECA (AZ MIT). Batch # ABW0411. Sealed

MODERNA (MOD). Batch # 3002183. Not sealed

JANSSEN (JAN). Batch # Not available. Not sealed.

<u>GRAPHENE PATTERN SAMPLES</u>

Reduced graphene oxide (rGO) (™Sigma Aldrich. Ref 805424)

GRAPHENE OXIDE Suspension (™The Graphene Box)

RAMAN spectrum of the reduced GRAPHENE OXIDE reference pattern (SIGMA ALDRICH™)

- For the rGO STANDARD the equipment shows thepresence of 3 characteristic peaks:
- G-band at 1584 cm^{-1}
- D-Band at 1344 cm^{-1}
- 2D-band at 2691 cm^{-1}
- In graphene oxide, the intensity of 2D is normally small with respect to G and D.
- Degree of disorder: I_D/I_G = 346/309 = 1.12
- Stacking level: I_{2D}/I_G = 219/309 = 0.70
- Previously, the equipment was calibrated with a silicon standard at 520 cm^{-1}

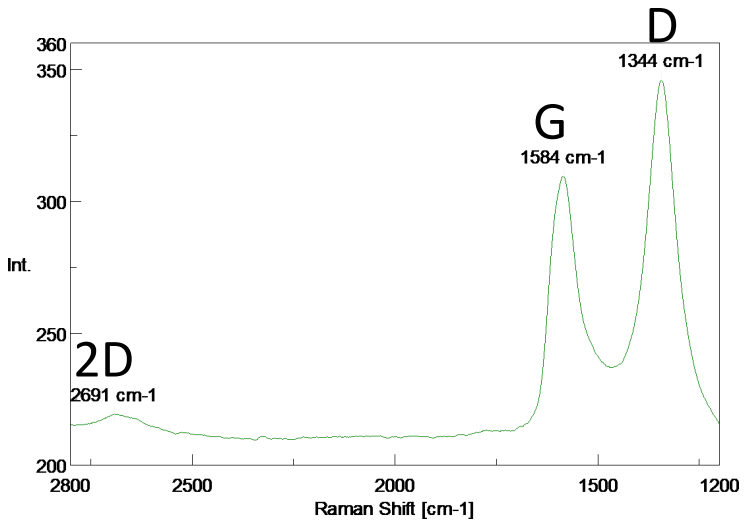

I_D/I_G=1.12

1.1. GROUP 1

OBJECTS WITH RAMAN SIGNAL SIMILAR TO THE REDUCED GRAPHENE OXIDE STANDARD

ANALYZED OBJECTS
GROUP 1

1. PFIZER 2 WBR UP GO2
2. PFIZER 3 ROS 2hy GO1b
3. PFIZER 3 ROS 2hy b GO2
4. PFIZER 3 ROS2 HY GO1
5. AZ MIT UP CARB 1
6. AZ MIT UP CARB4
7. AZ MIT DOWN CARB2
8. MOD lump1

1. PFIZER 2
WBR UP GO2

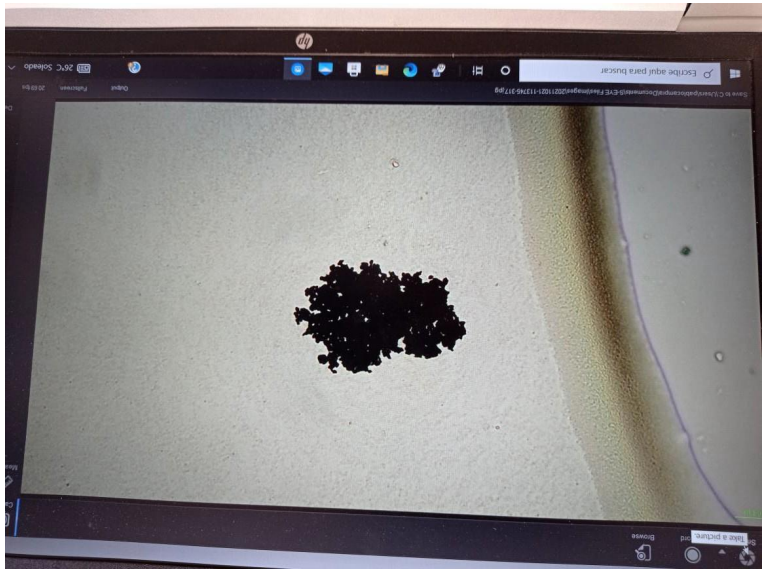

1. PFIZER 2
WBR UP GO2

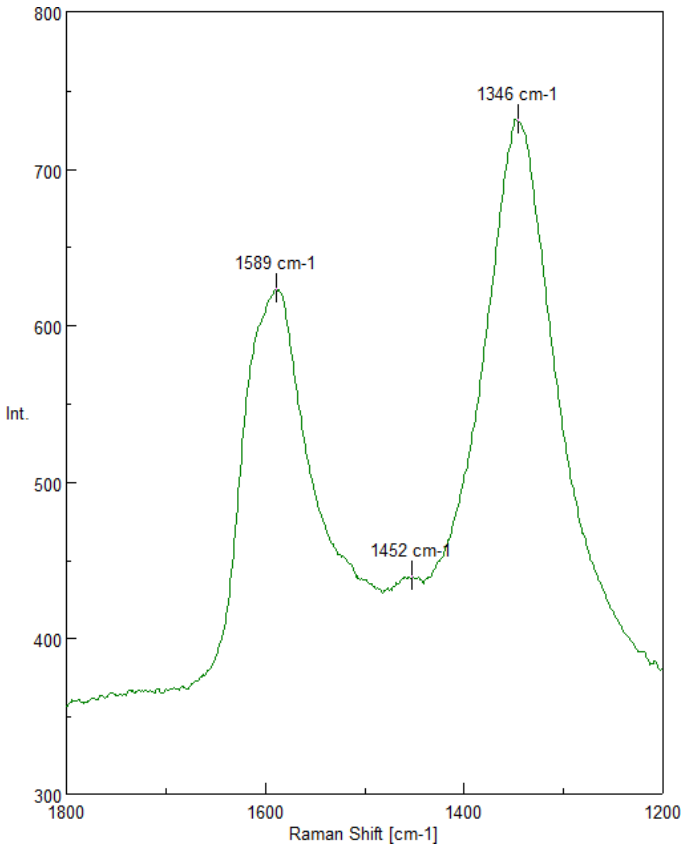

$I_D/I_G = 1.18$

2. PFIZER 3
ROS 2 HY GO1

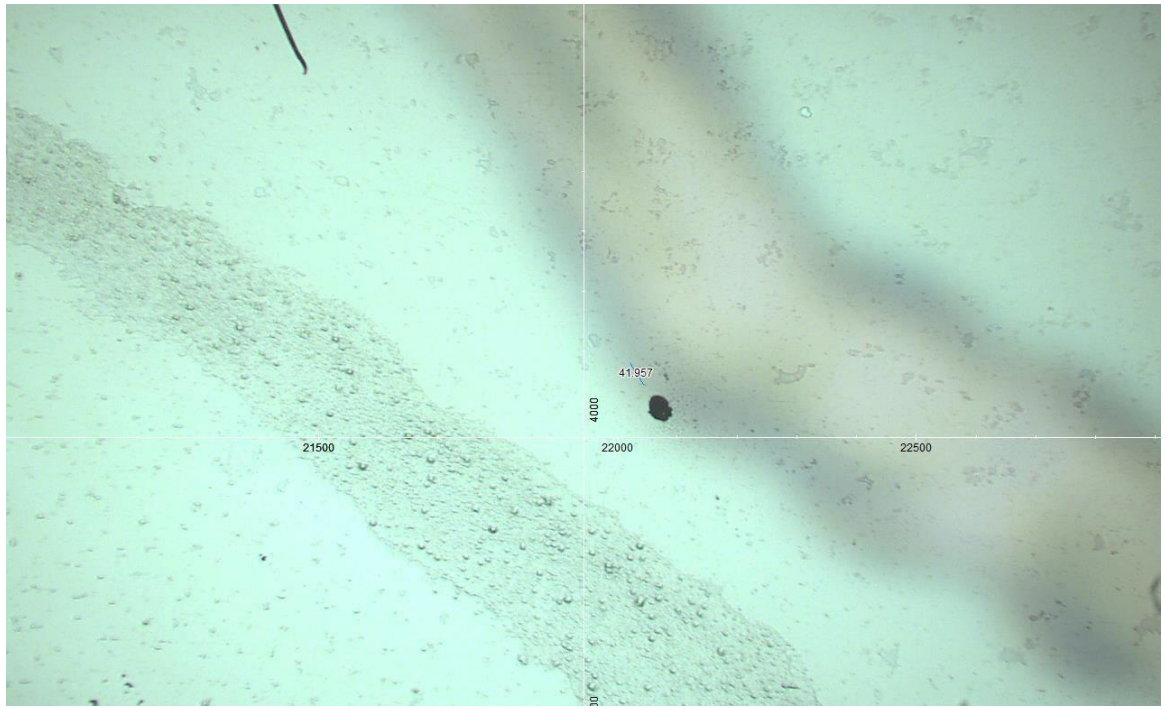

2. PFIZER 3
ROS 2 HY GO1

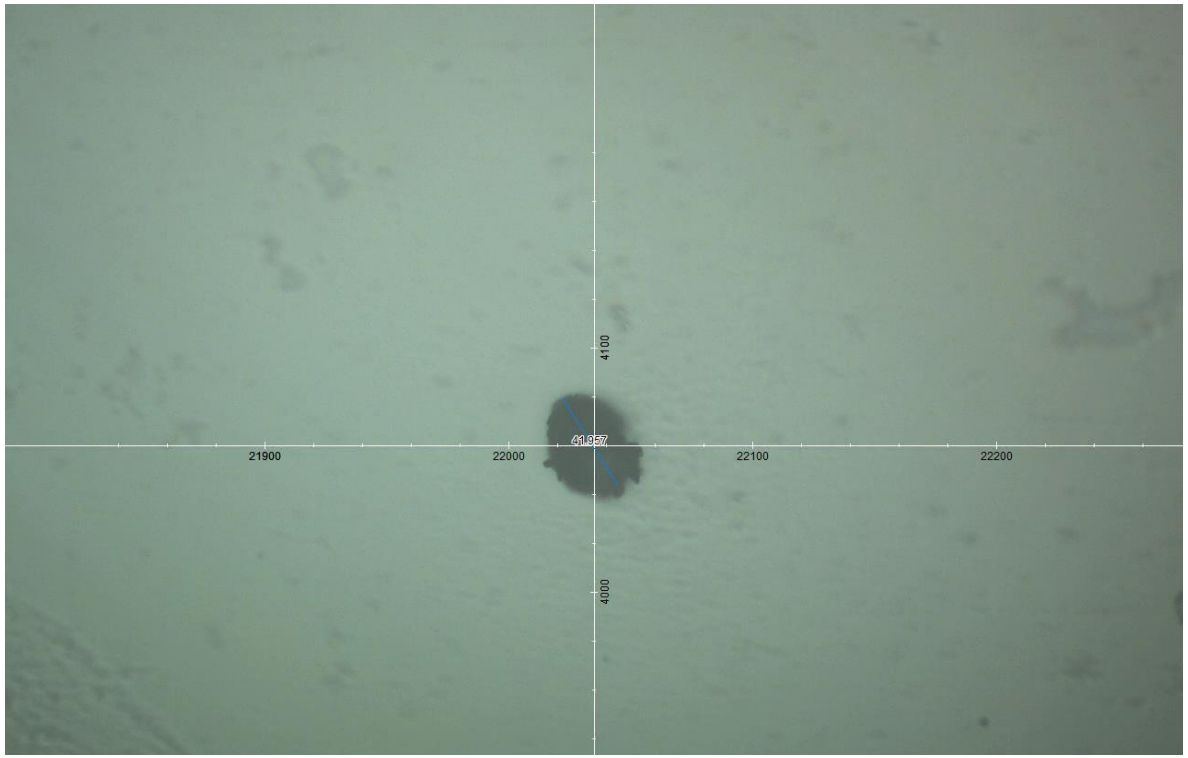

2. PFIZER 3
ROS 2 HY GO1

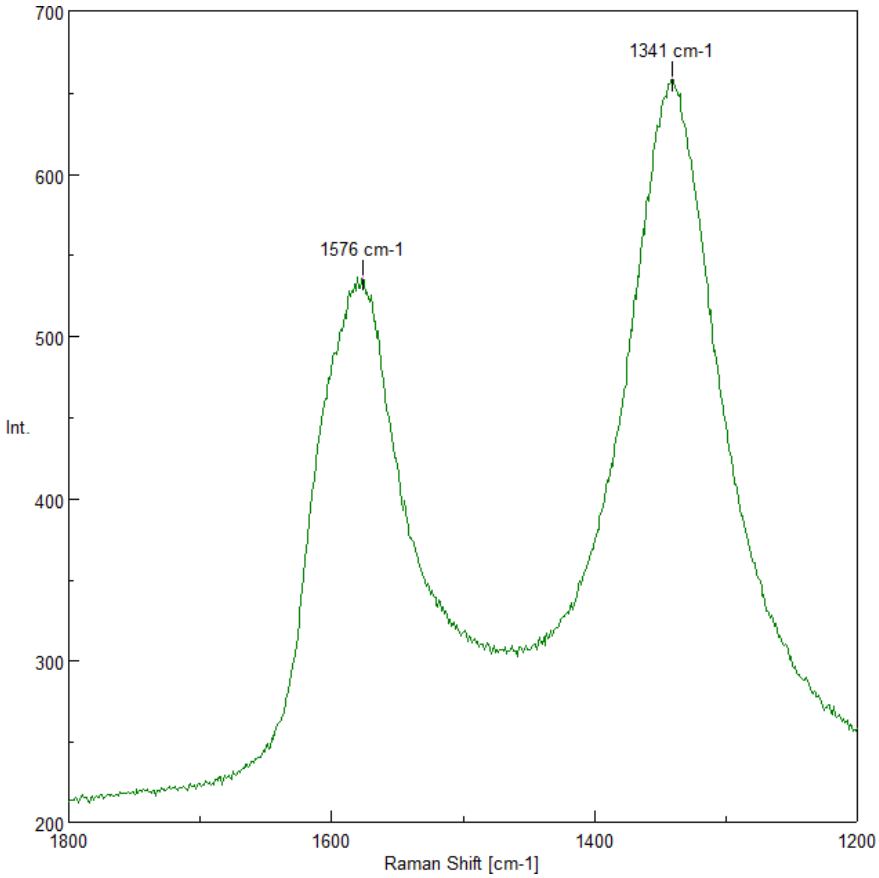

$I_D/I_G = 1.22$

3. PFIZER 3
Ros 2hy GO1b

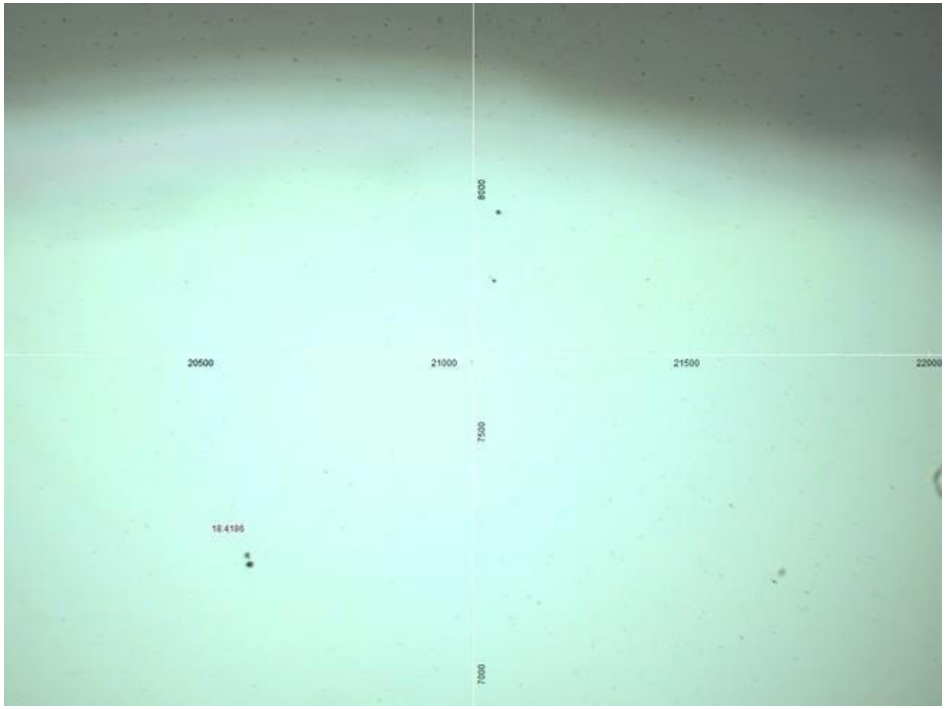

3. PFIZER 3
Ros 2hy GO1b

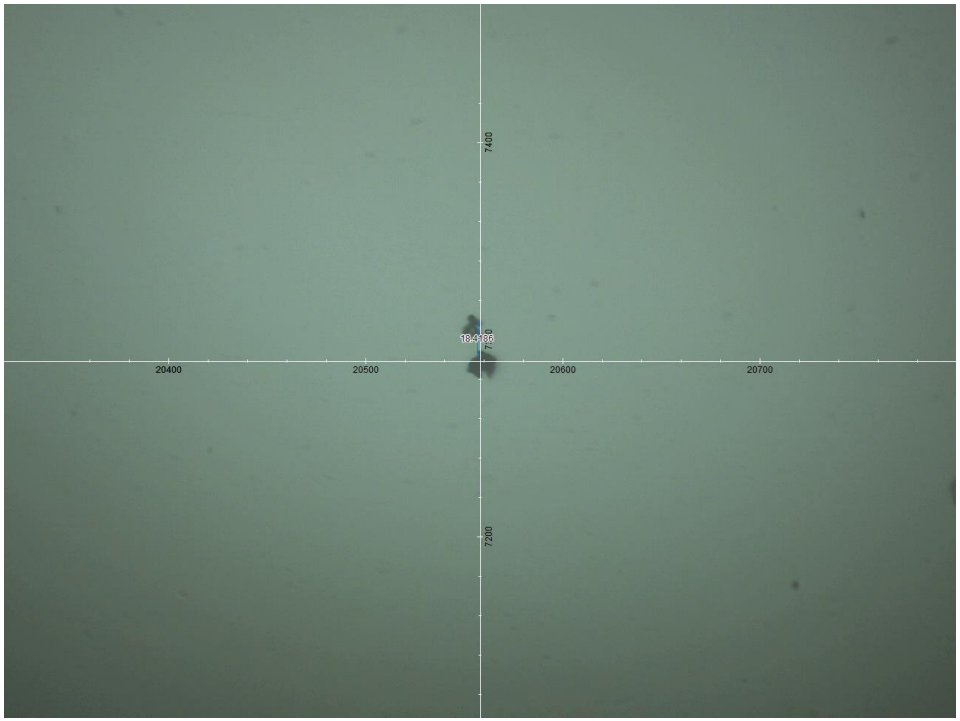

3. PFIZER 3 Ros 2hy GO1b

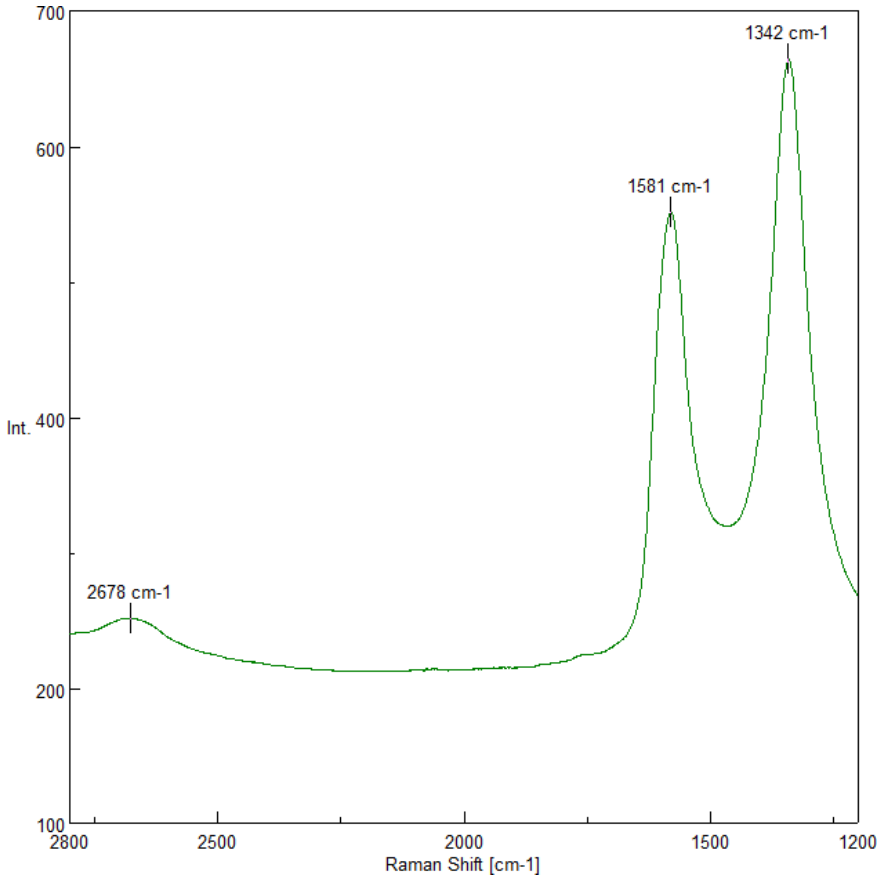

$I_D/I_G = 1.22$

4. PFIZER 3
Ros 2hy b GO2

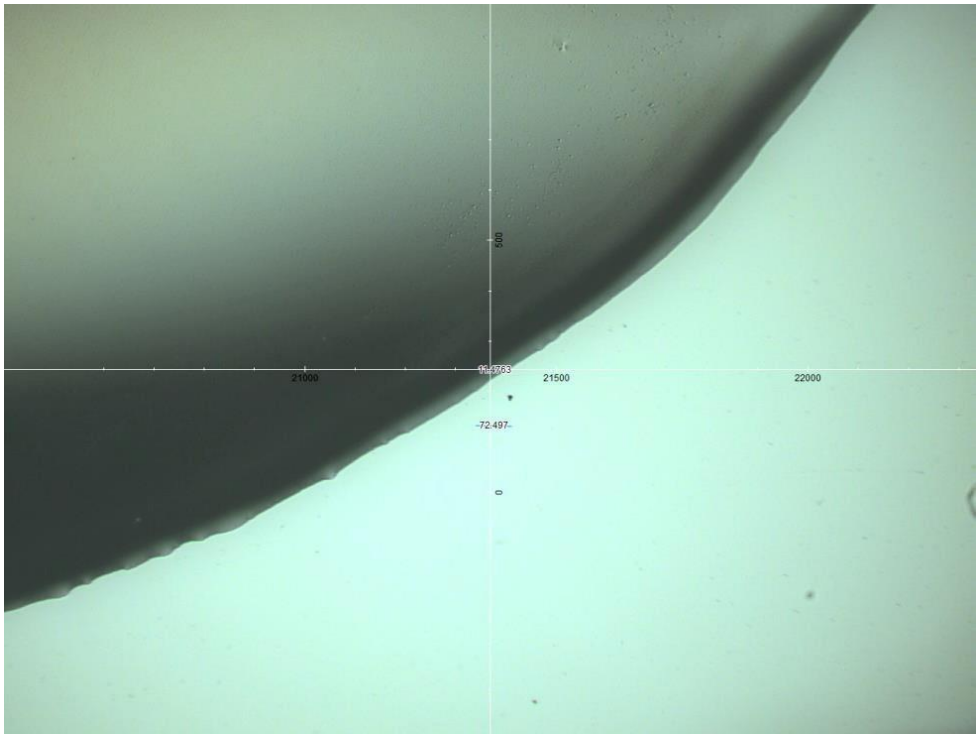

4. PFIZER 3
Ros 2hy b GO2

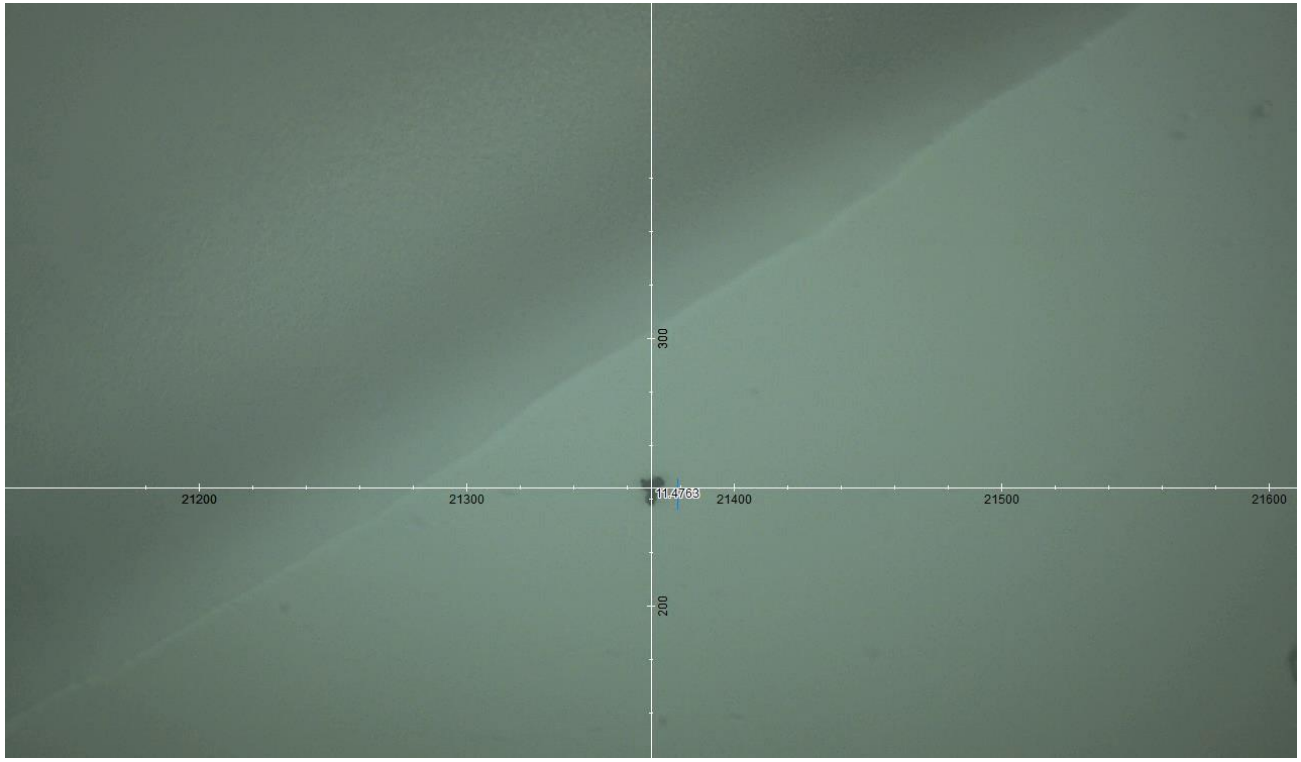

4. PFIZER 3
Ros 2hy b GO2

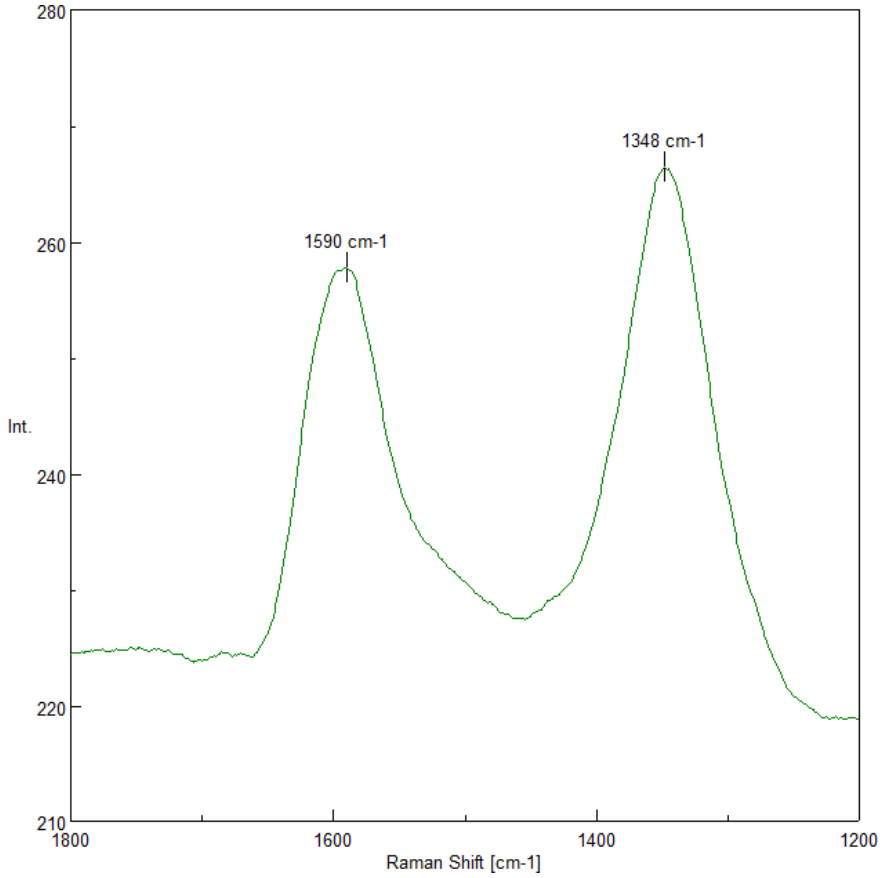

$I_D/I_G = 1.03$

5. ASTRAZENECA
AZ MIT UP CARB1

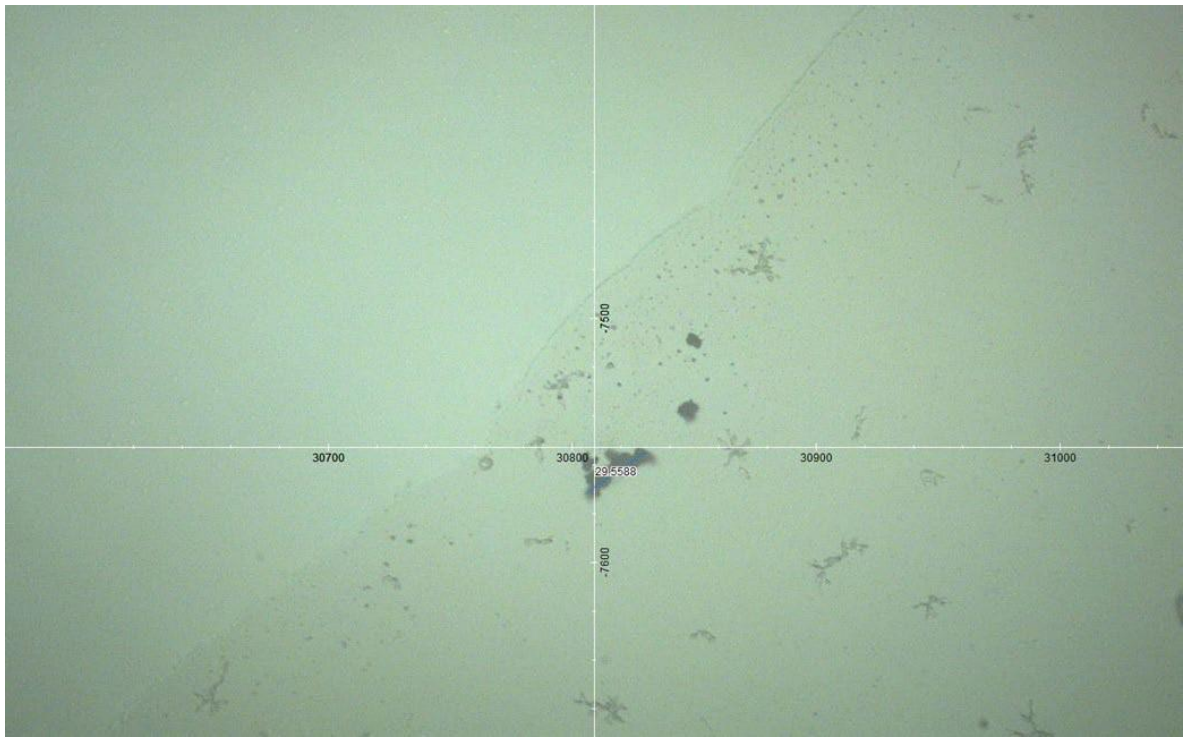

5. ASTRAZENECA
AZ MIT UP CARB1

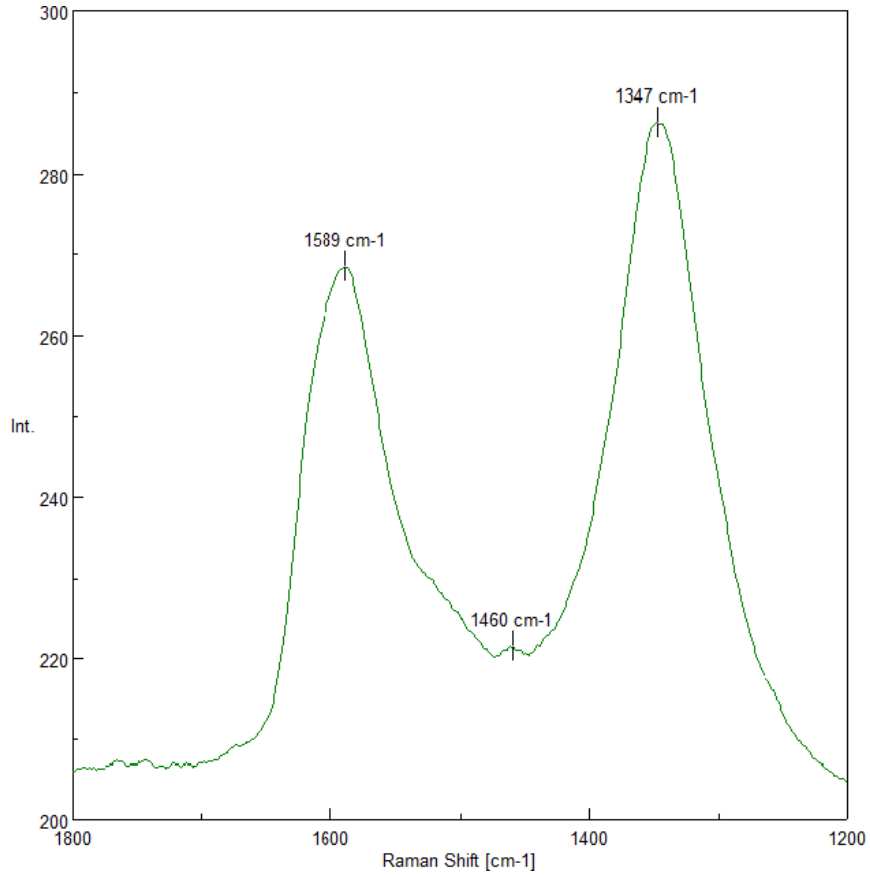

$I_D/I_G = 1.07$

6. ASTRAZENECA
AZ MIT UP CARB4

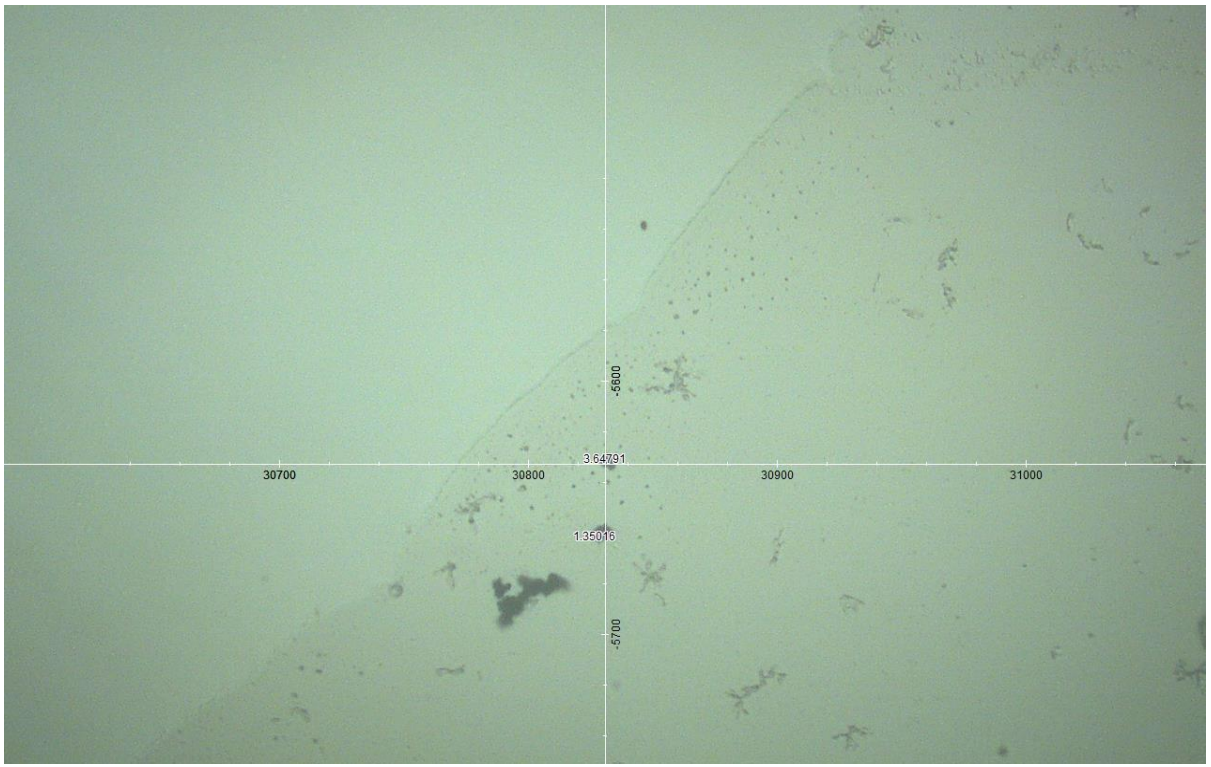

6. ASTRAZENECA
AZ MIT UP CARB4

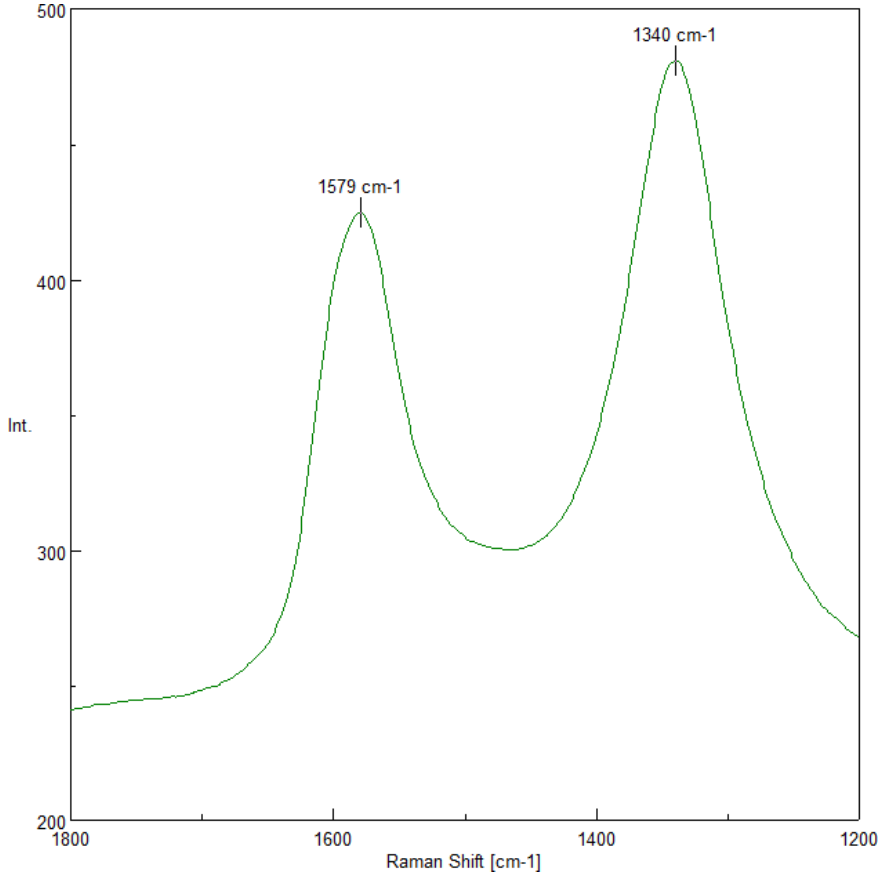

$I_D/I_G = 1.14$

7. ASTRAZENECA
AZ MIT DOWN 2 CARB2

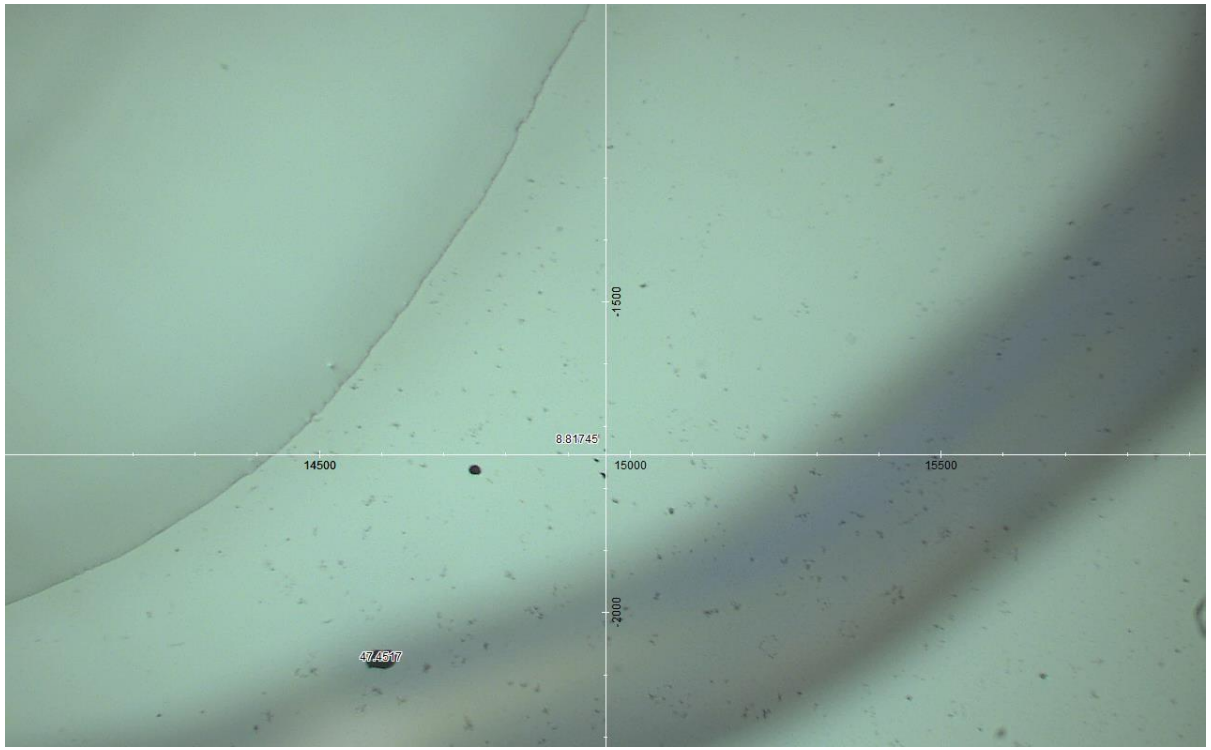

7. ASTRAZENECA
AZ MIT DOWN 2 CARB2

$I_D/I_G = 1.18$

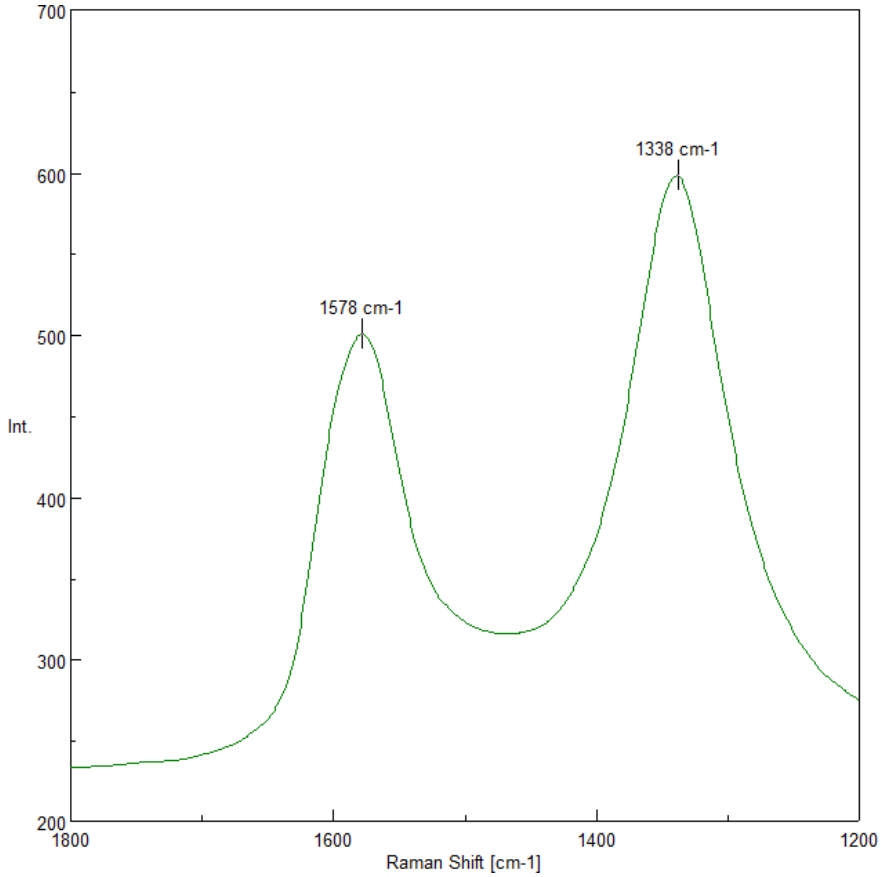

8. MODERNA
MOD lump1

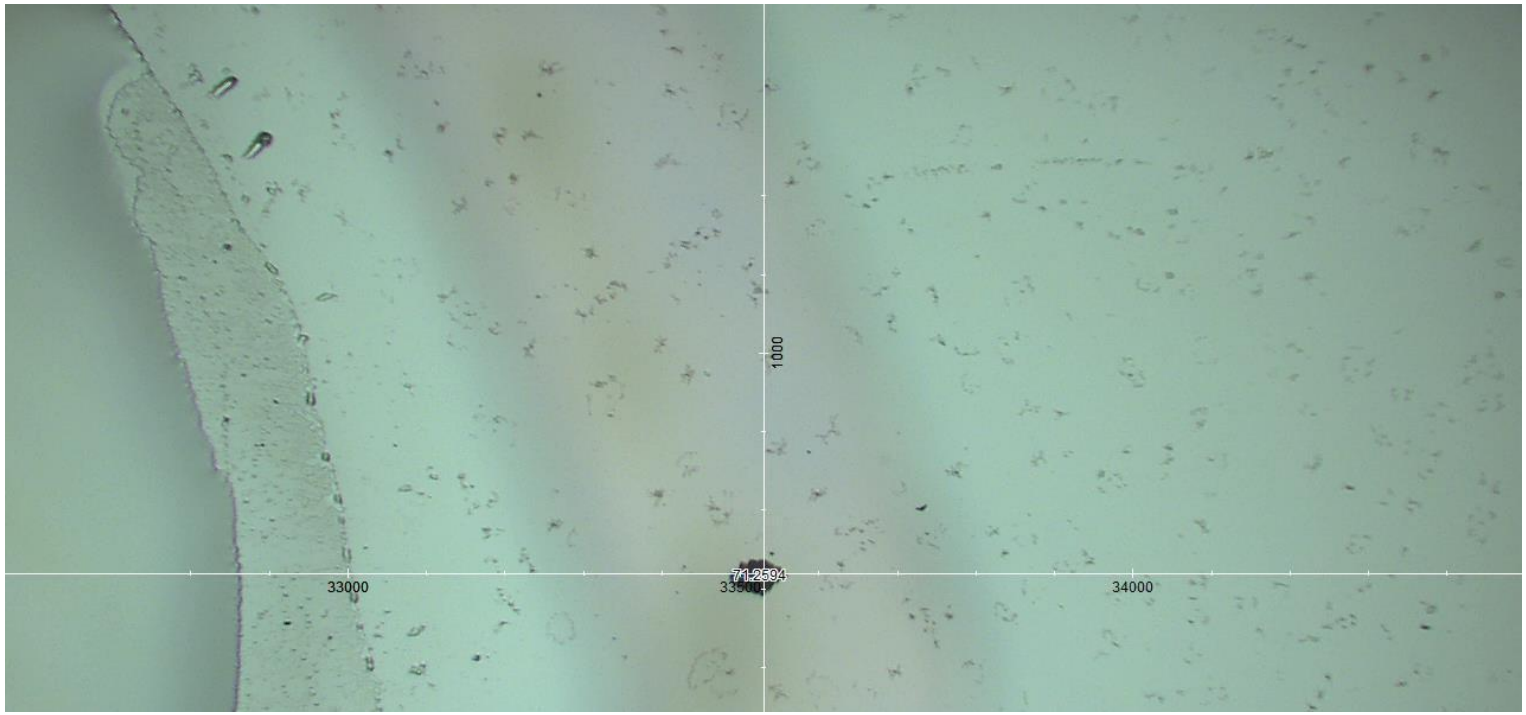

8. MODERNA
MOD lump1

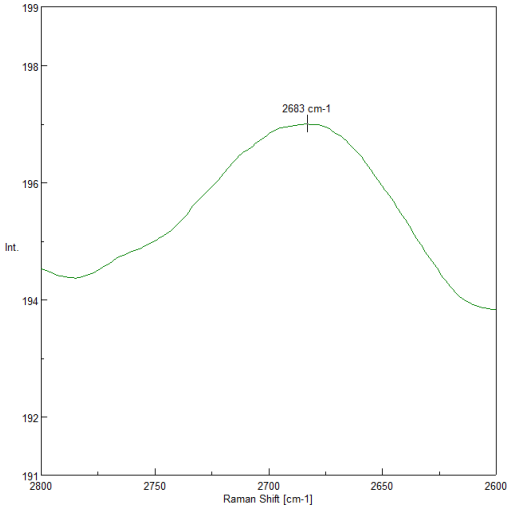

$I_D/I_G = 1.11$

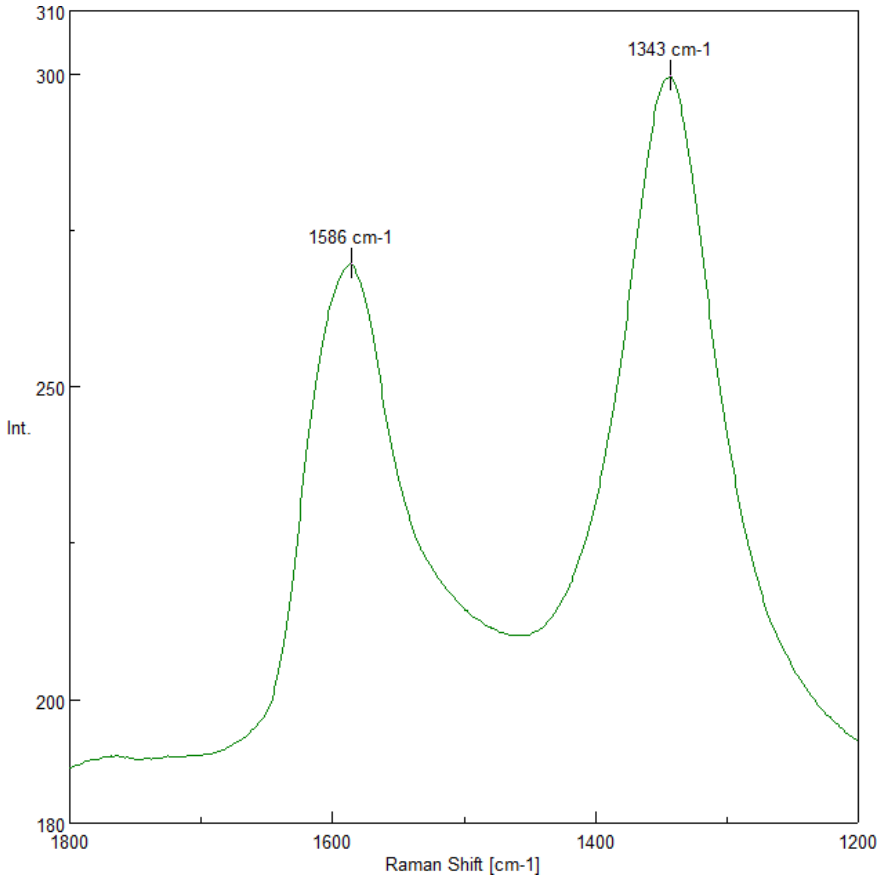

1.2. GROUP 2:

OBJECTS WITH SIGNALS COMPATIBLE WITH GRAPHITE OR GRAPHENE DERIVATIVES

ANALYZED OBJECTS
GROUP 2

9 PFIZER 2 WBR GO1
10 PFIZER 2 WBR GO6a
11 PFIZER 2 WBR 2 GO7
12 PFIZER 2 WBR UP GO1
13 PFIZER 2 WBR UP GO3b
14 PFIZER 2 WBR UP GO4
15 PFIZER 2 WBR DOWN GO2
16 PFIZER 2 WBR DOWN GO3
17 PFIZER 2 WBR DOWN GO5
18 PFIZER 3 ROS OBJ 1
19 PFIZER 3 ROS 2 OBJ 1
20 PFIZER 3 ROS 2 OBJ 2

21 PFIZER 4 Pdown lump1
22 PFIZER 4 Pdown lump2
23 PFIZER 4 Pdown lump3
24 ASTRAZENECA AZ MIT UP CARB5
25 ASTRAZENECA AZ MIT UP CARB6
26 JANSSEN JAN GO1
27 JANSSEN JAN GO3
28 JANSSEN JAN GO4

9. PFIZER 2
WBR GO1

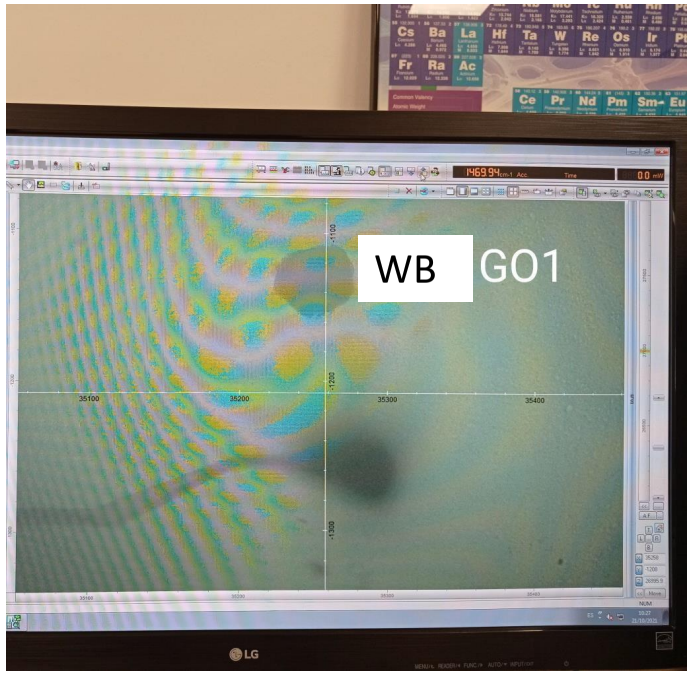

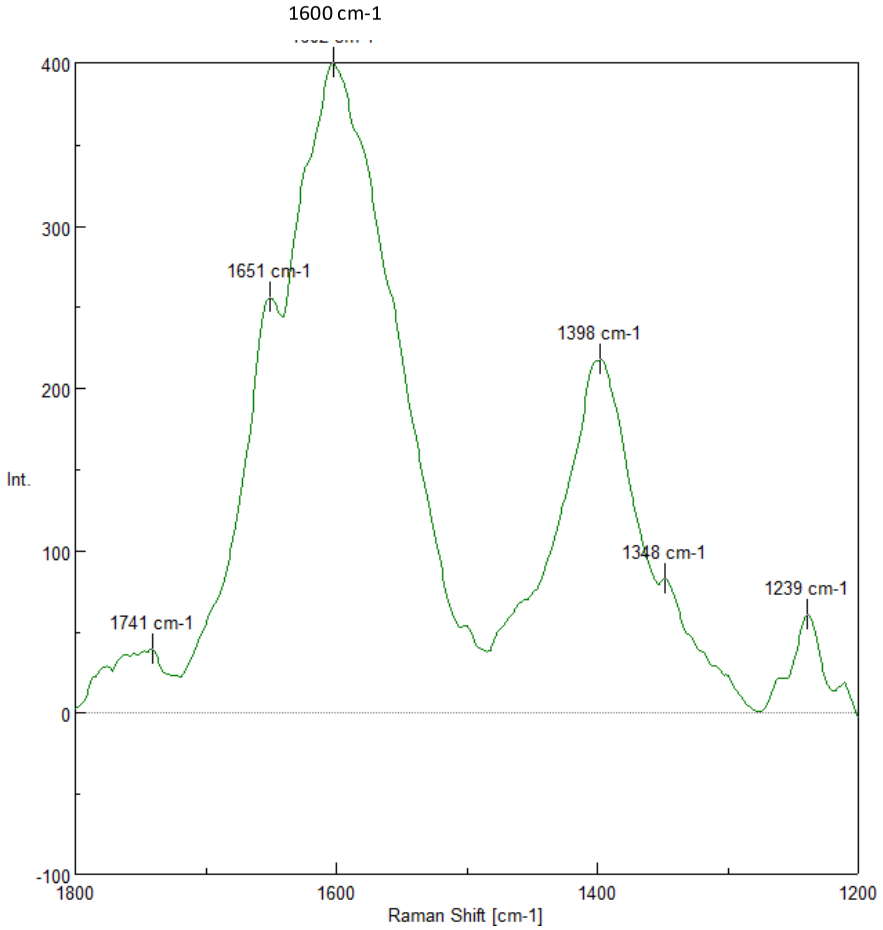

28. PFIZER 2
WBR GO6a

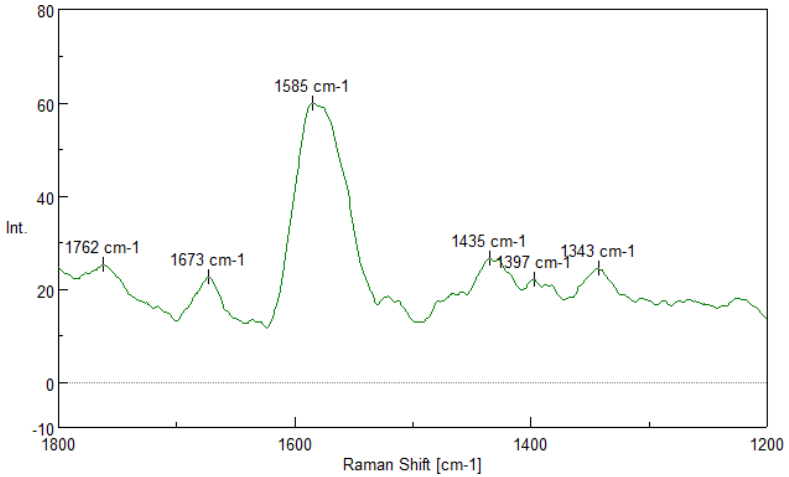

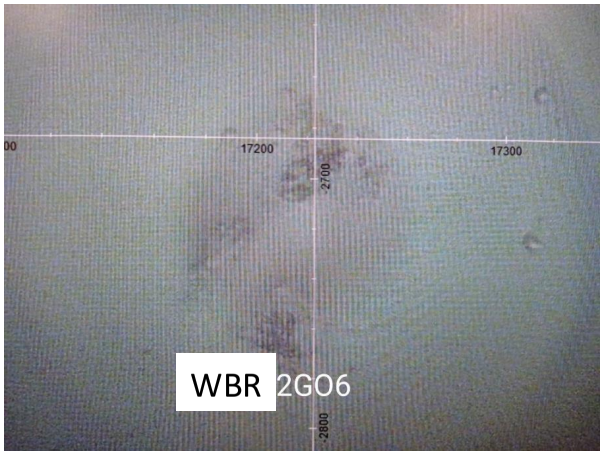

11. PFIZER 2
WBR2 GO7

11. PFIZER 2
WBR GO 7

I_D/I_G = 0.48

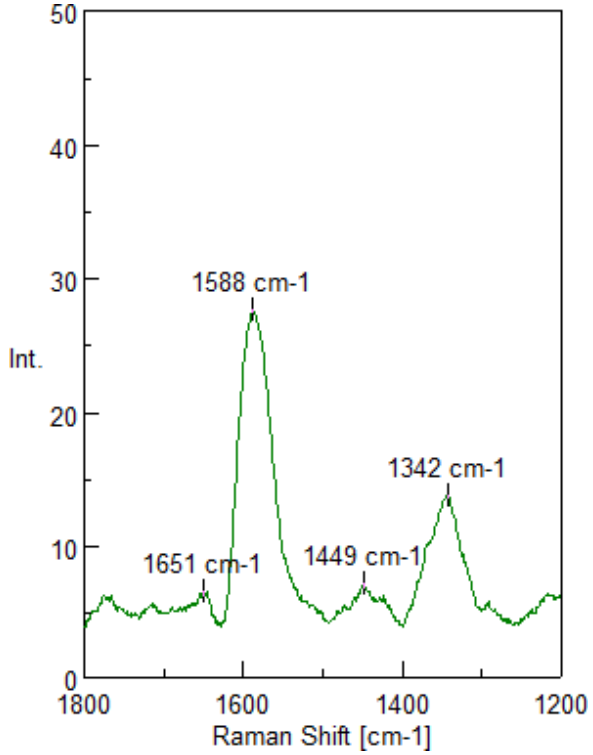

11. PFIZER 2 WBRGO7(1200-2800cm^{-1})

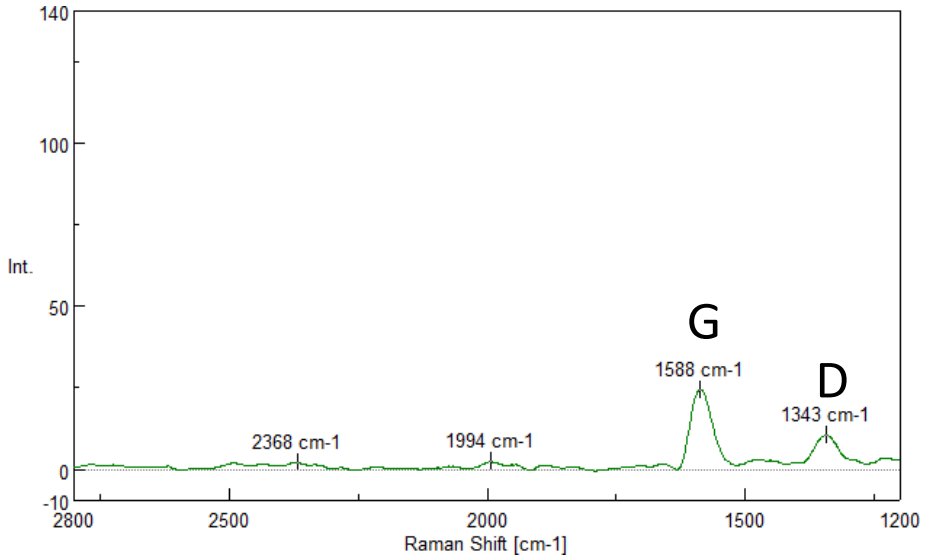

12. PFIZER 2
WBR UP GO1

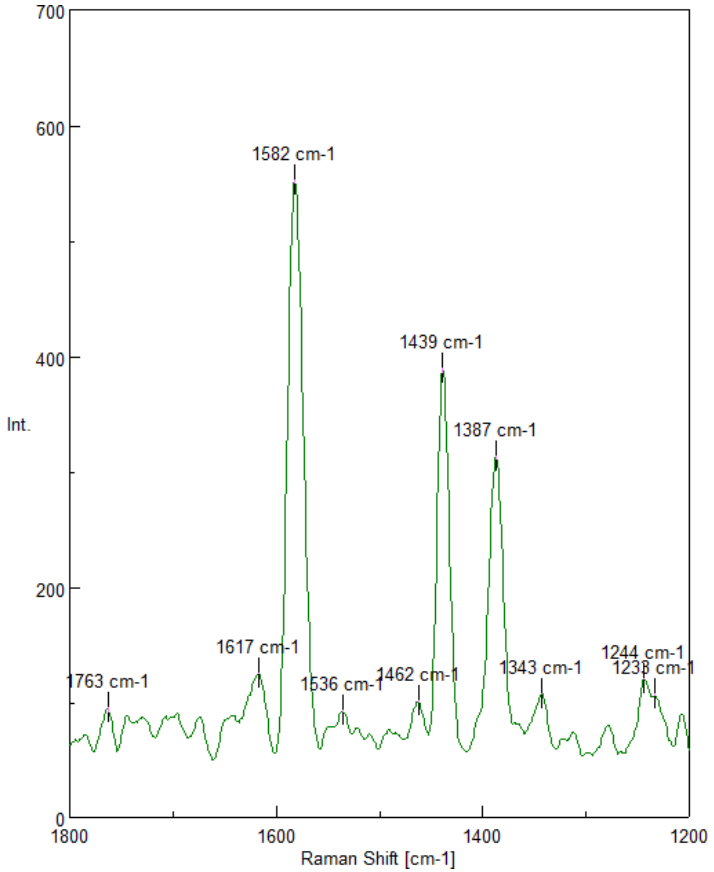

13. PFIZER
WBR UP GO3b

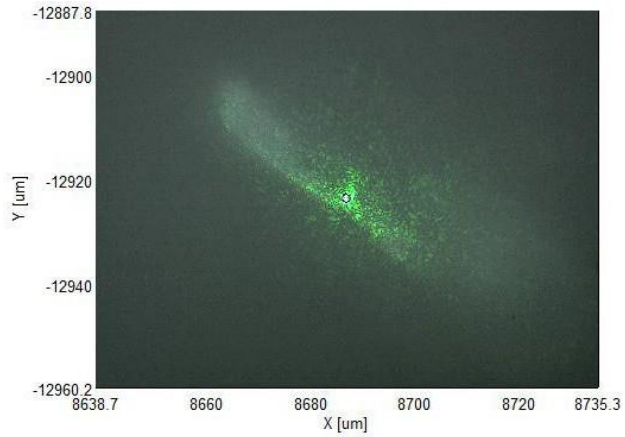

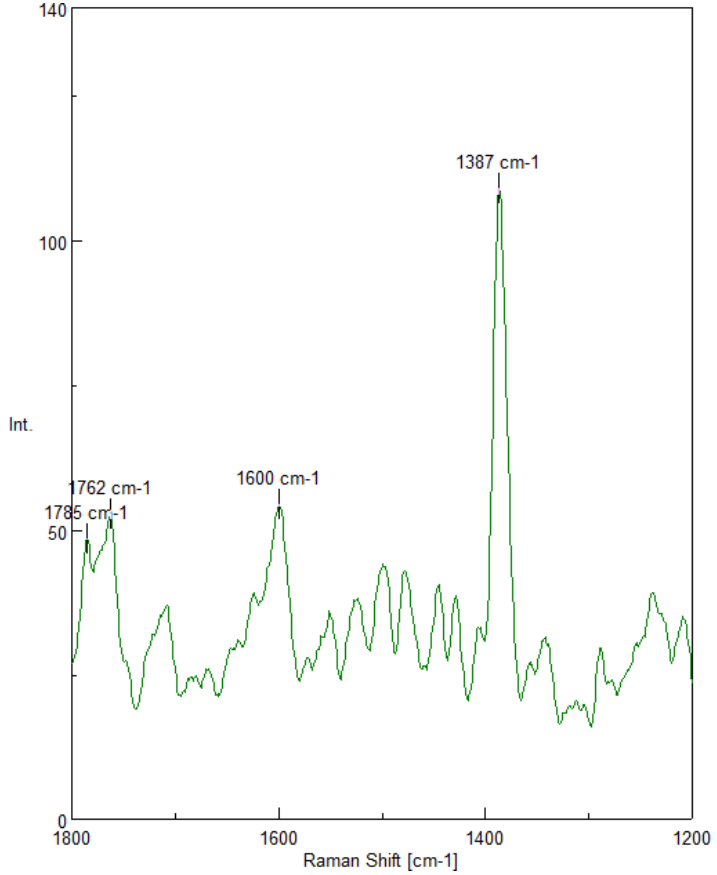

14. PFIZER 2
WBR UP GO4

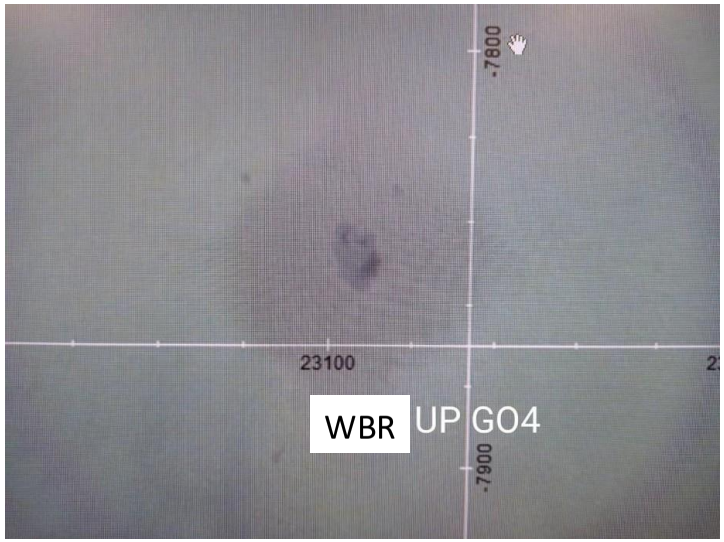

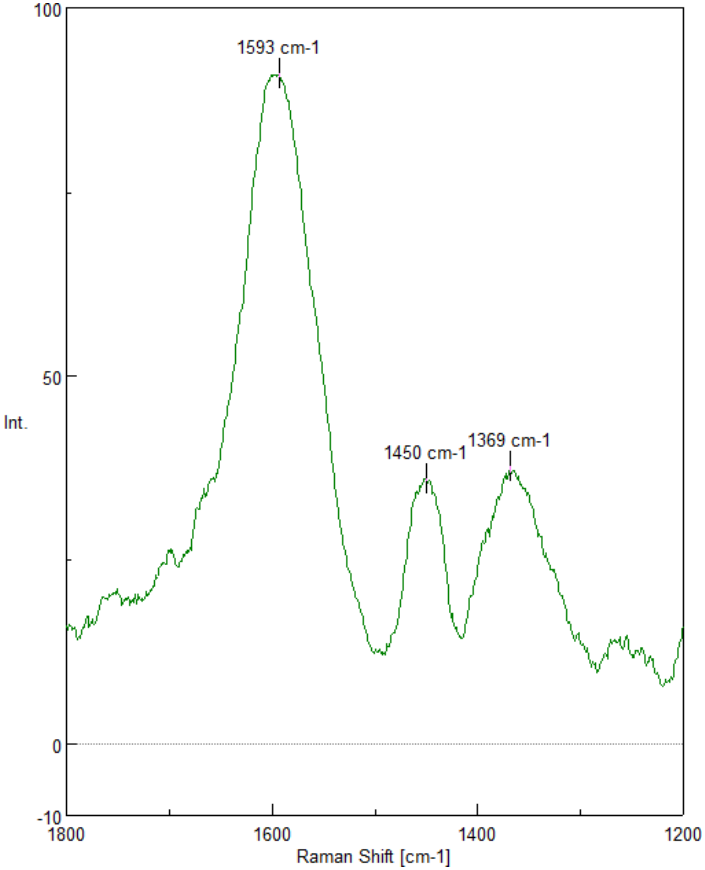

15. PFIZER 2
WBR DOWN GO2

Photo N/A

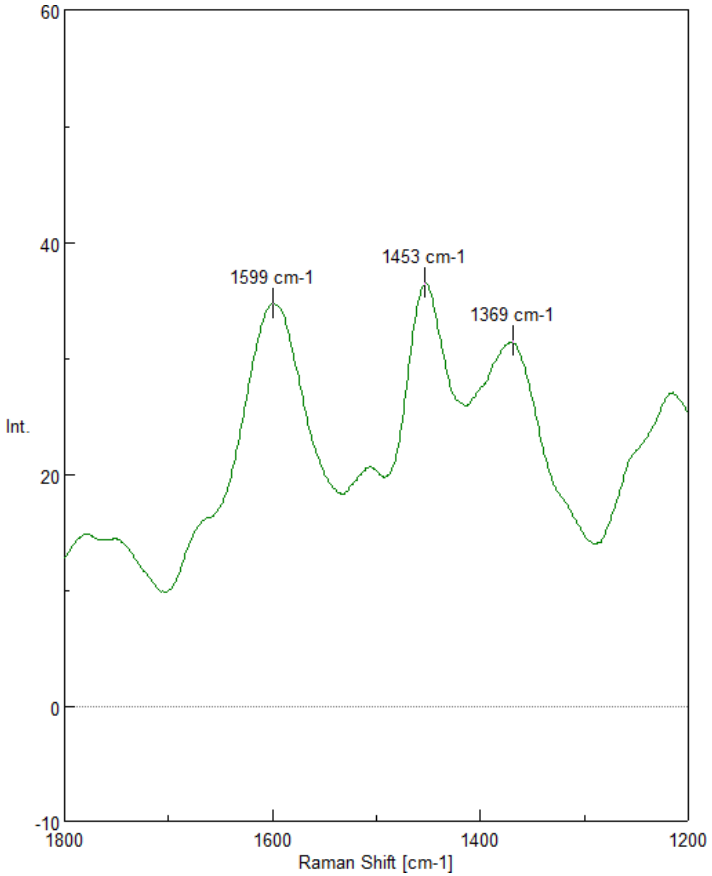

16. FIZER 2
WBR DOWN GO3

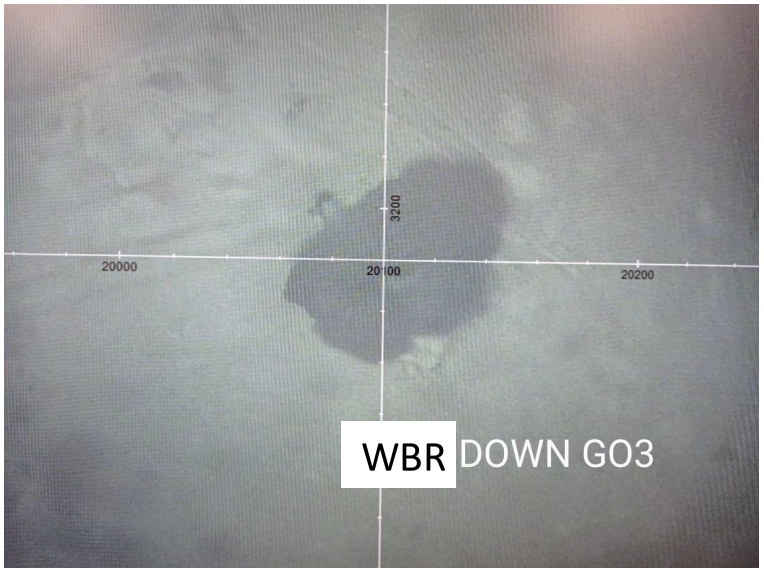

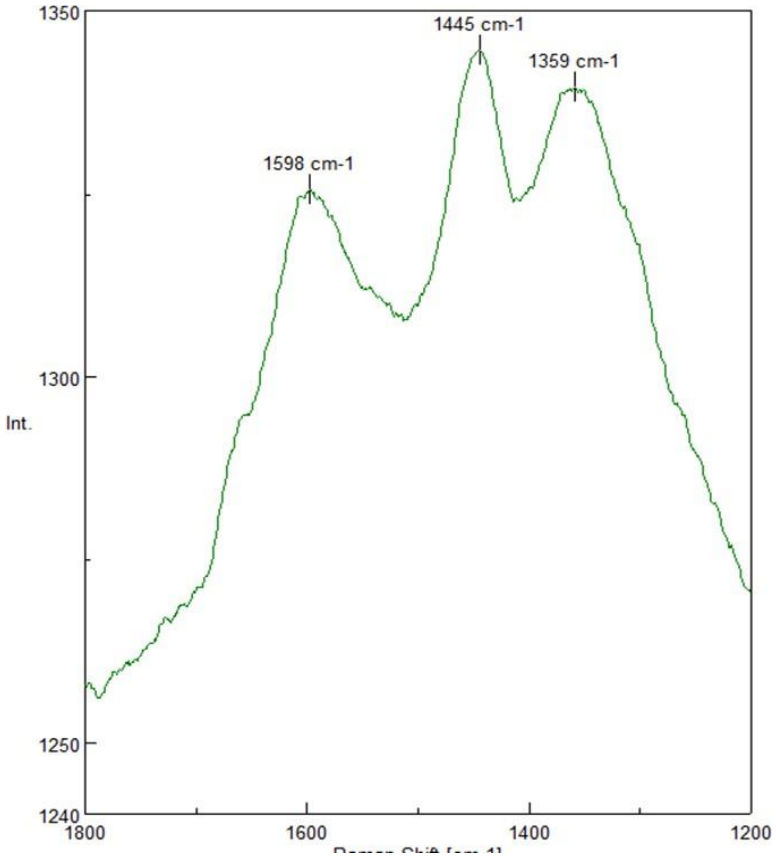

17. PFIZER 2
WBR DOWN GO5

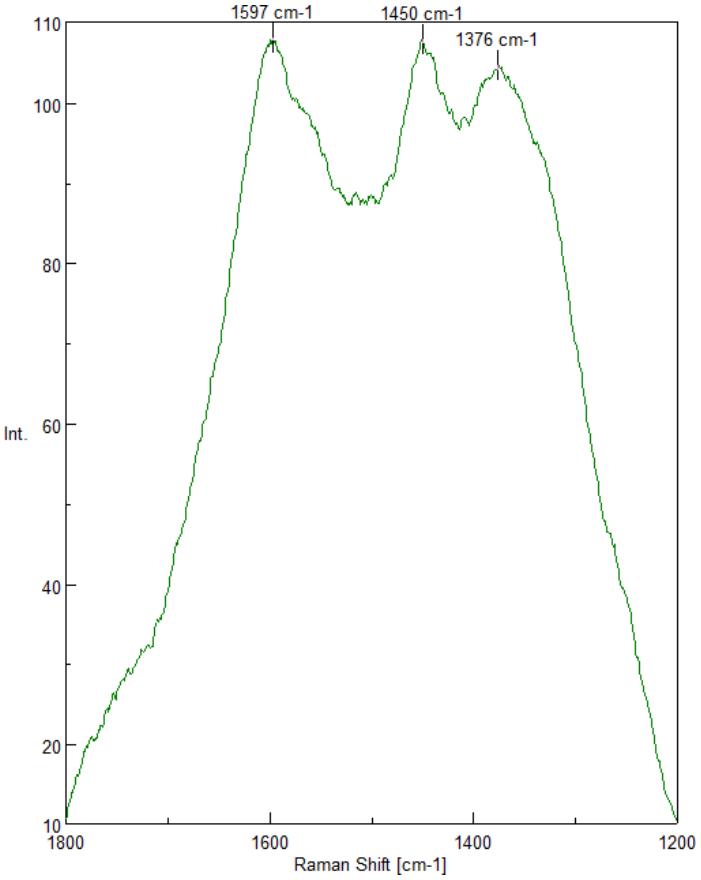

18. PFIZER 3
Ros OBJ 1

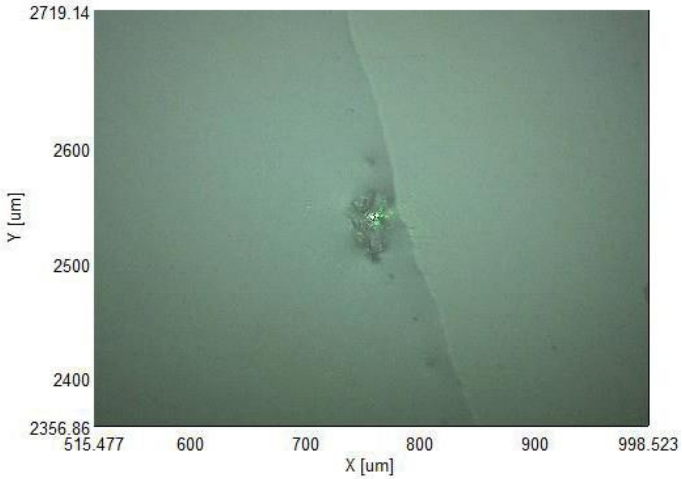

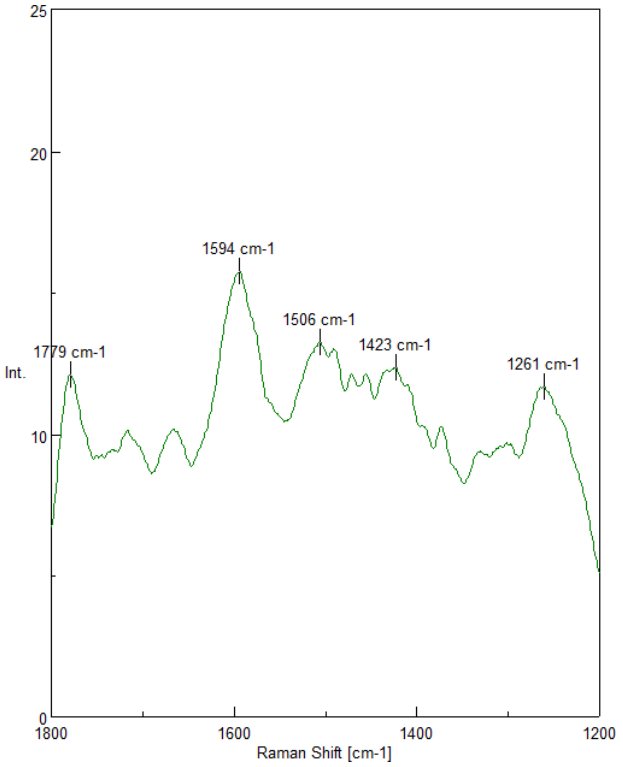

19. PFIZER 3
ROS 2 OBJ 1

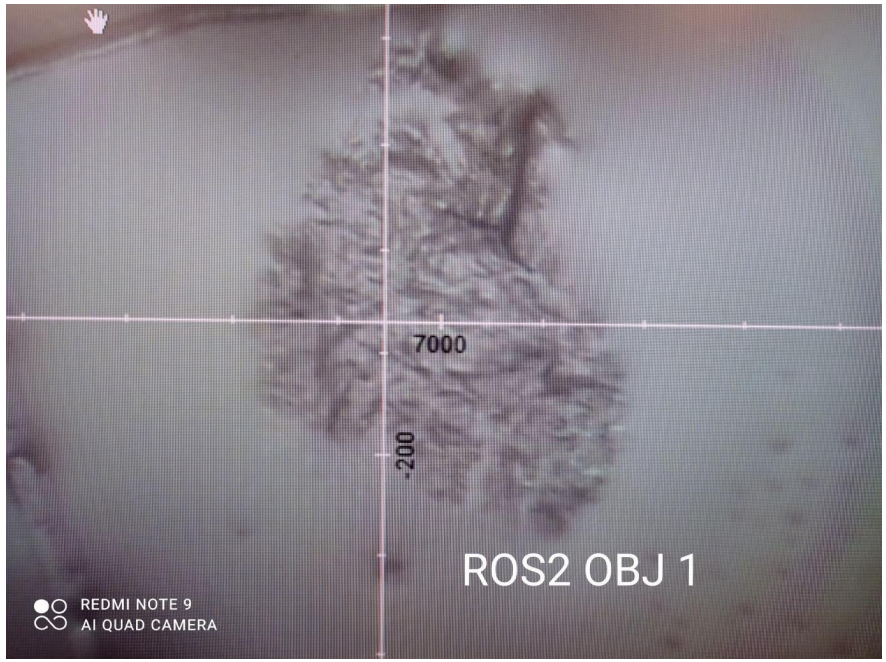

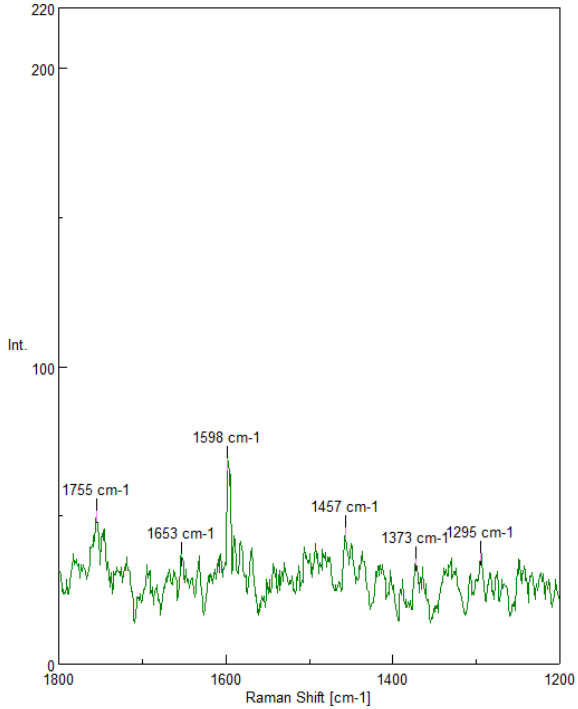

20. PFIZER 3
ROS 2 OBJ2

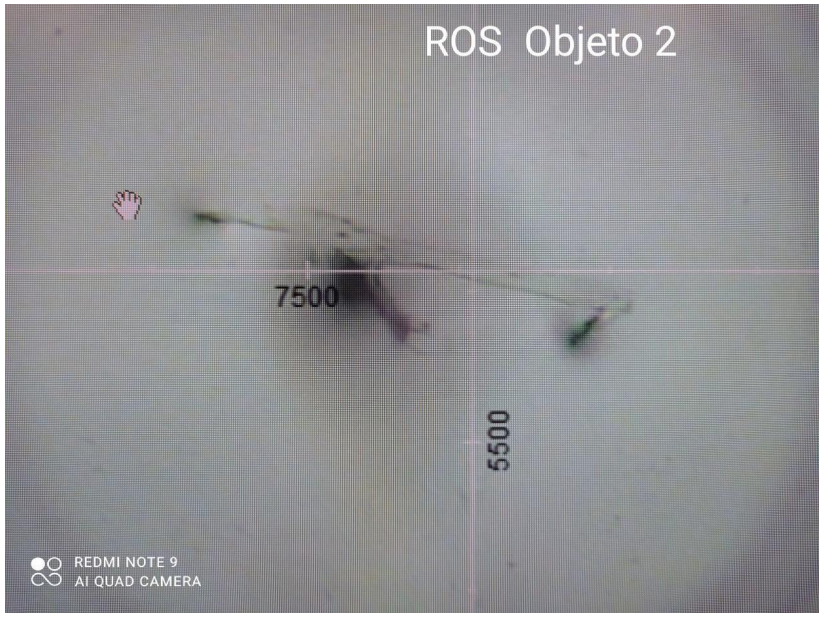

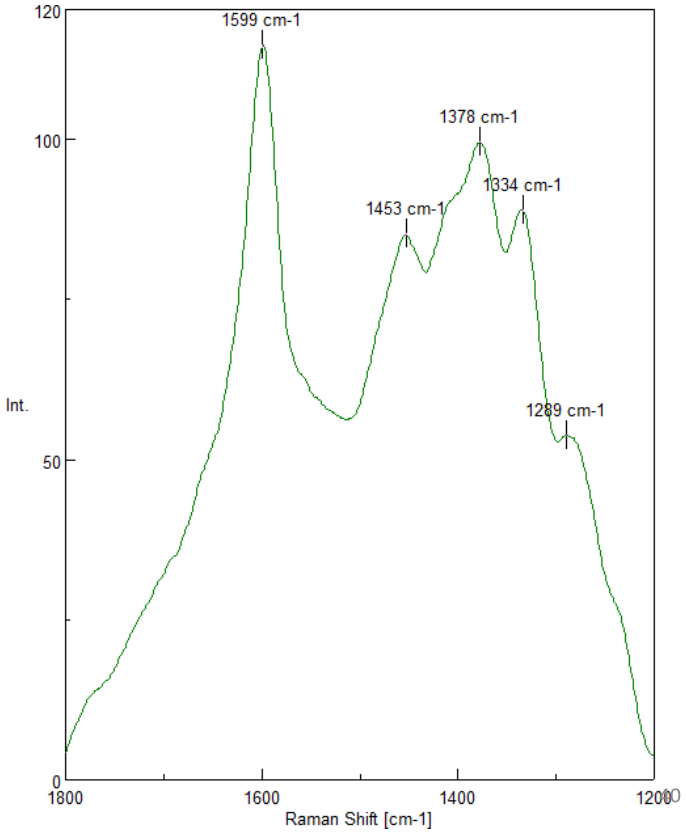

21. PFIZER 4: Pdown lump1

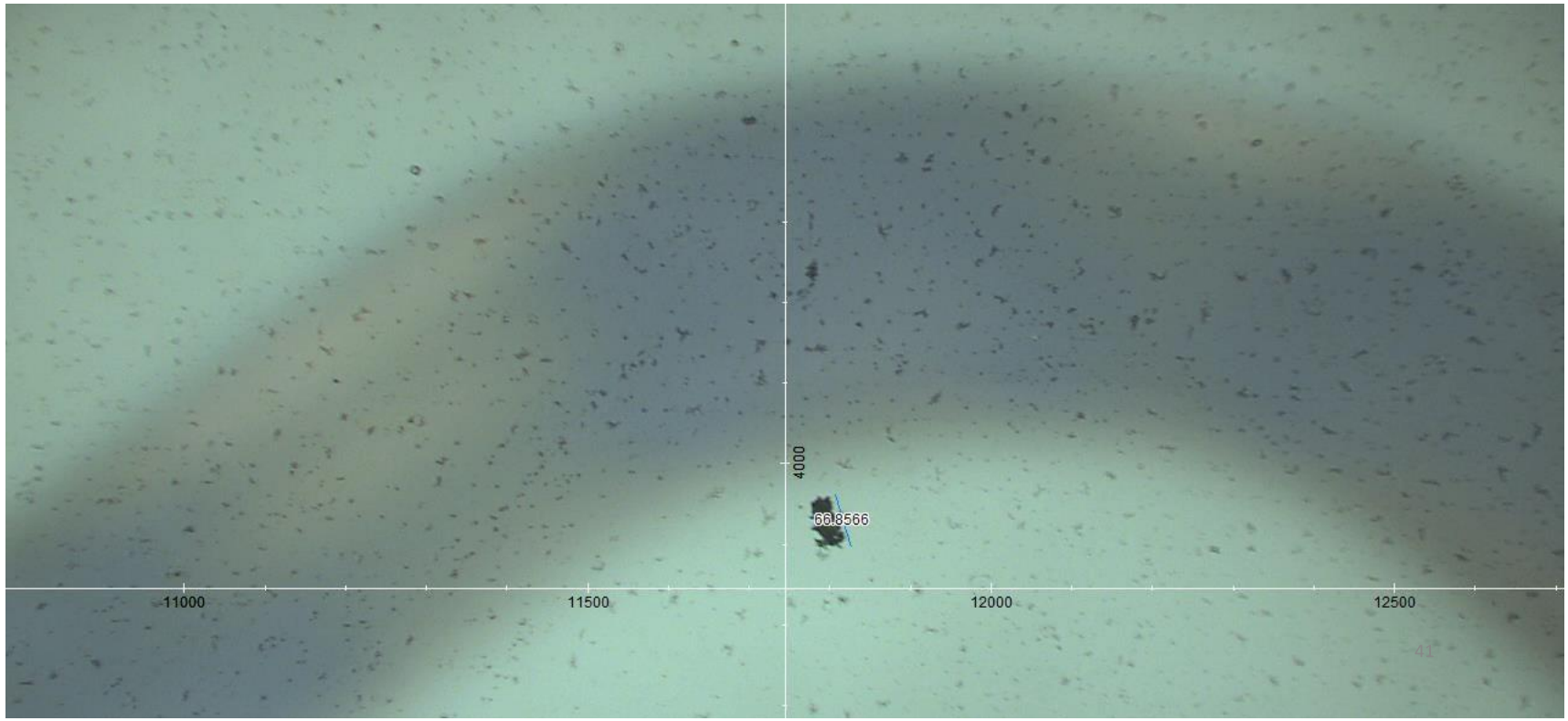

21. PFIZER 4: Pdown lump1

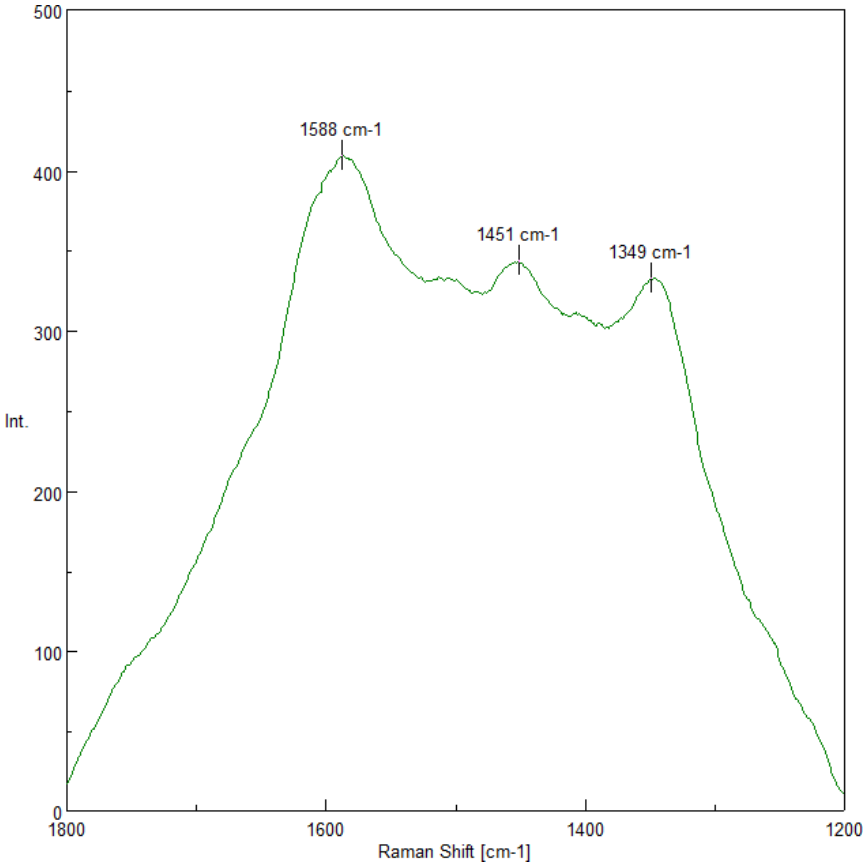

22. PFIZER 4

Pdown lump2

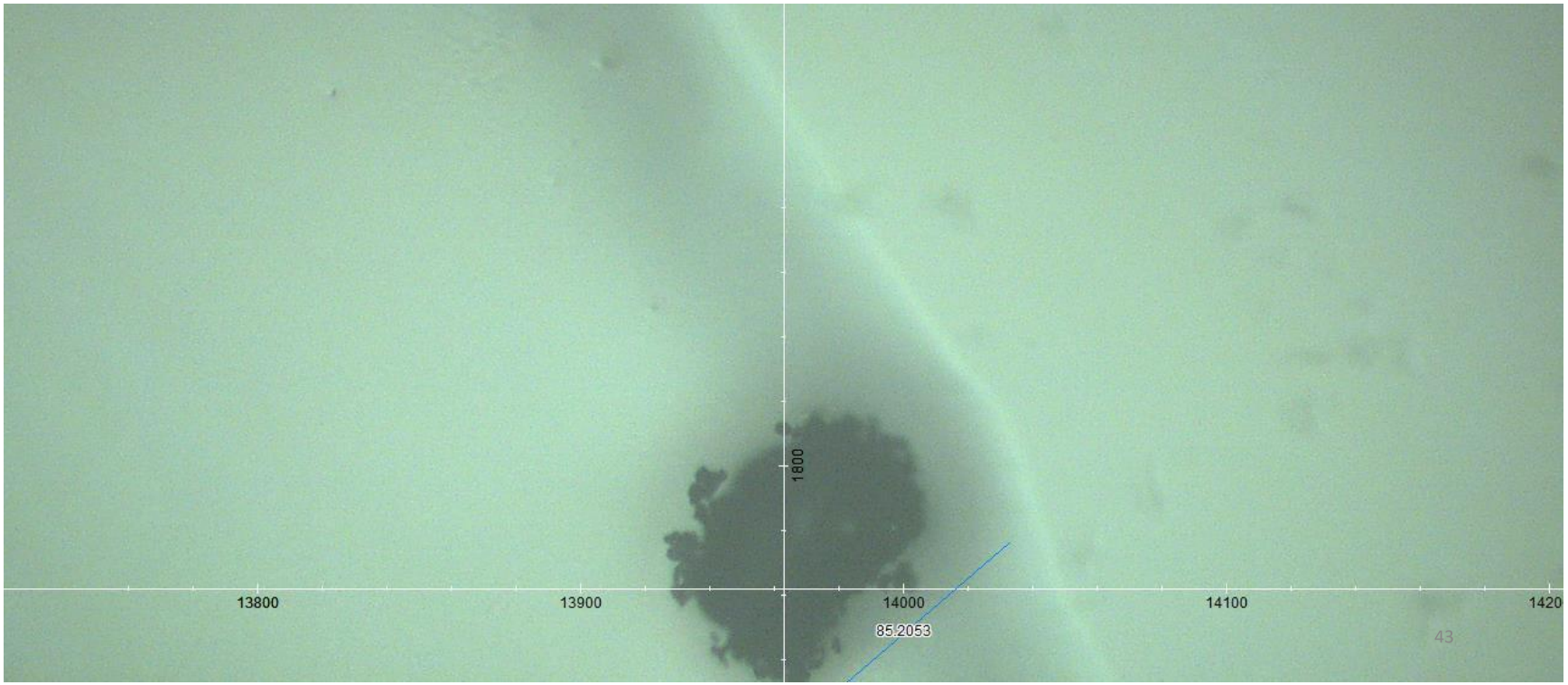

43

22. PFIZER 4
Pdown lump2

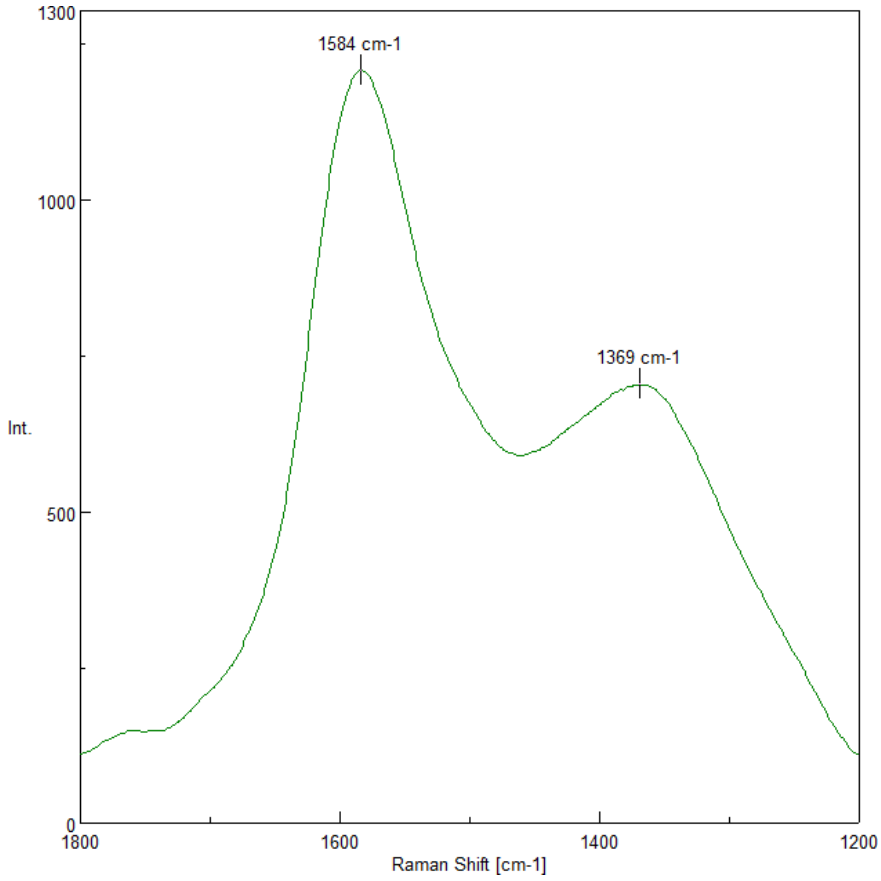

$I_D/I_G = 0.58$

23. PFIZER 4
Pdown lump3

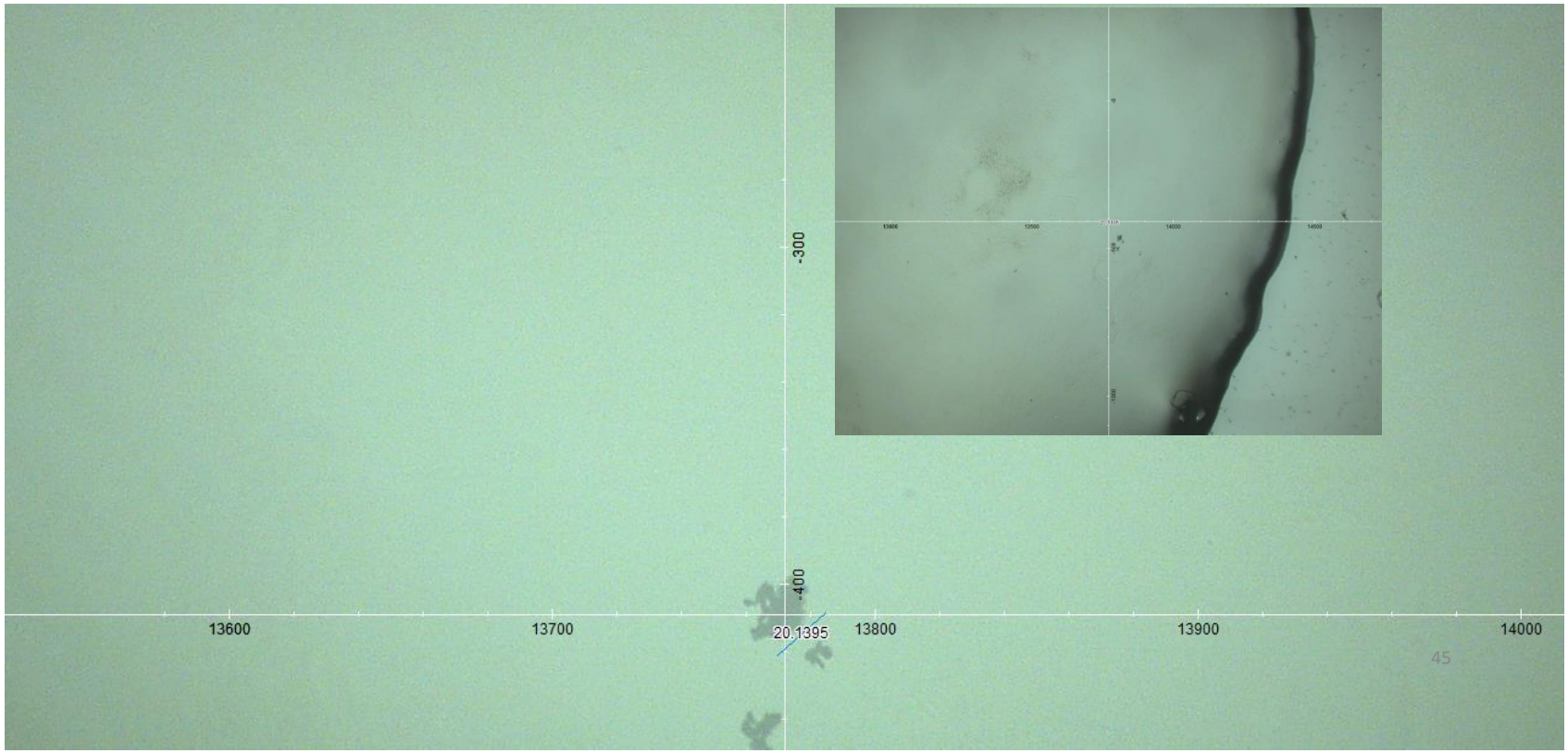

45

23. PFIZER 4 Pdown lump3

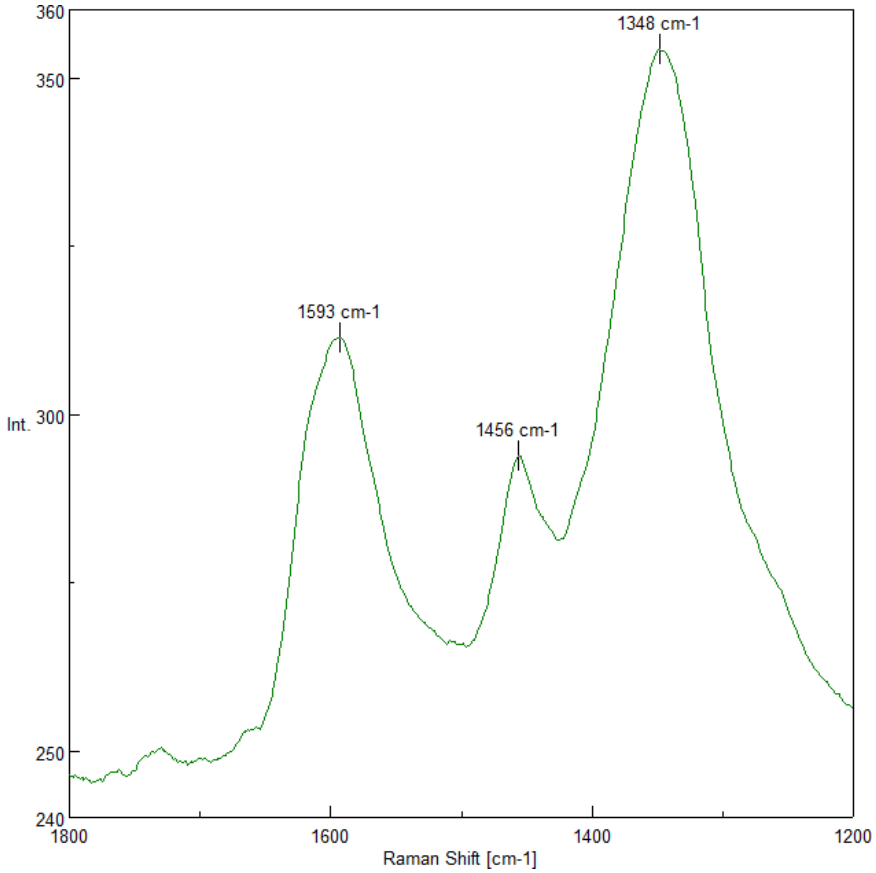

24. ASTRAZENECA
AZ MIT UP CARB5

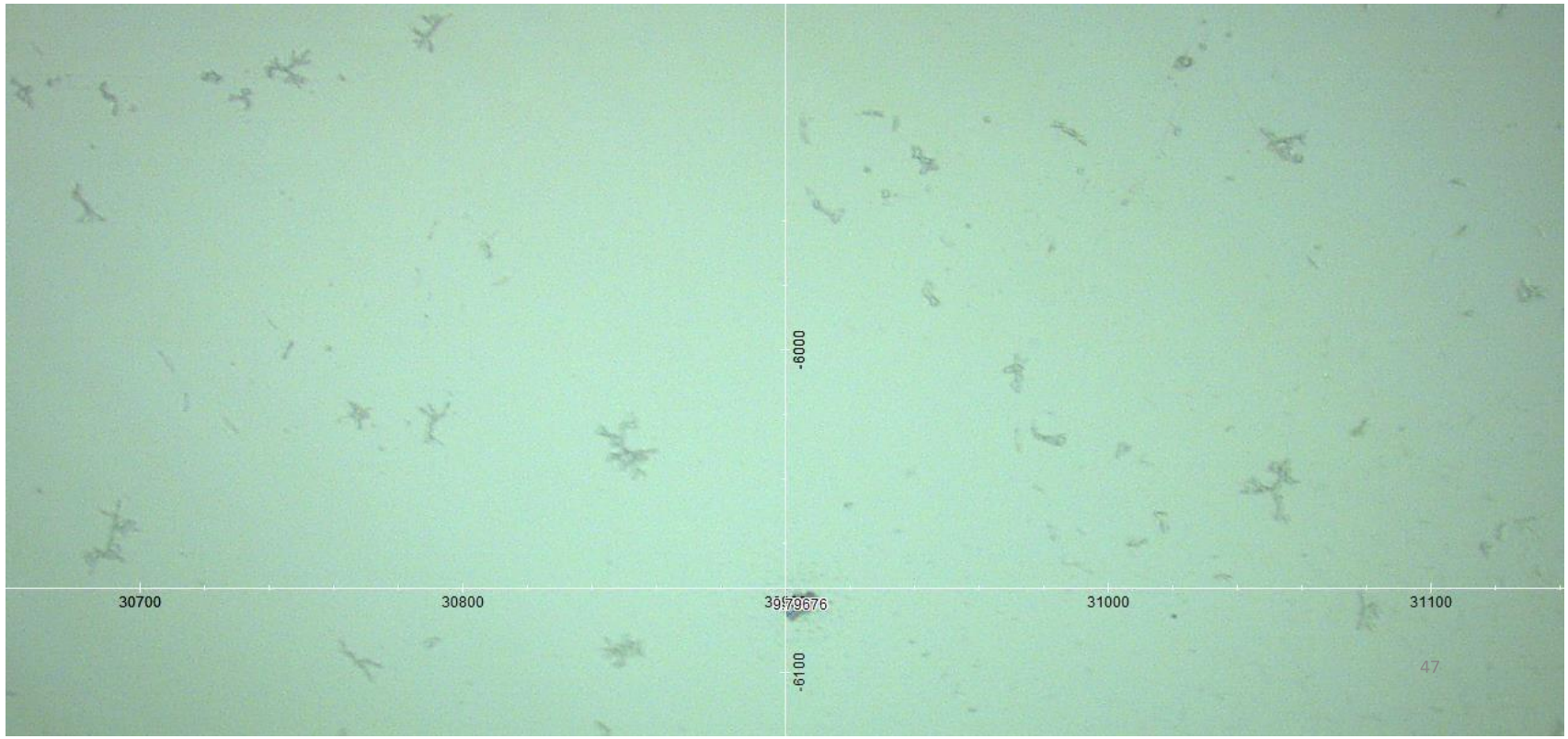

24. ASTRAZENECA AZ MIT UP CARB5

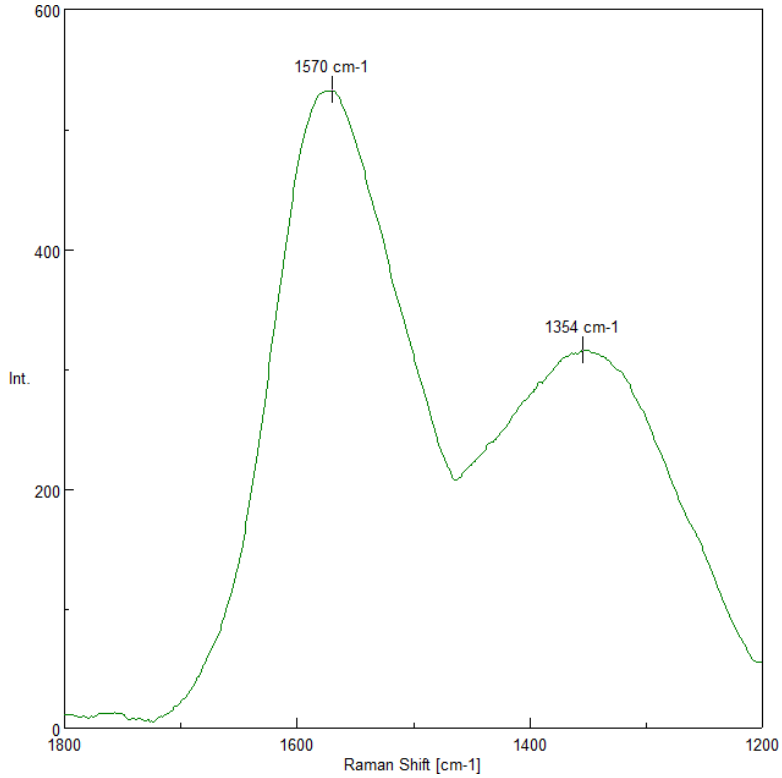

$I_D/I_G = 0.59$

25. ASTRAZENECA
AZ MIT UP CARB6

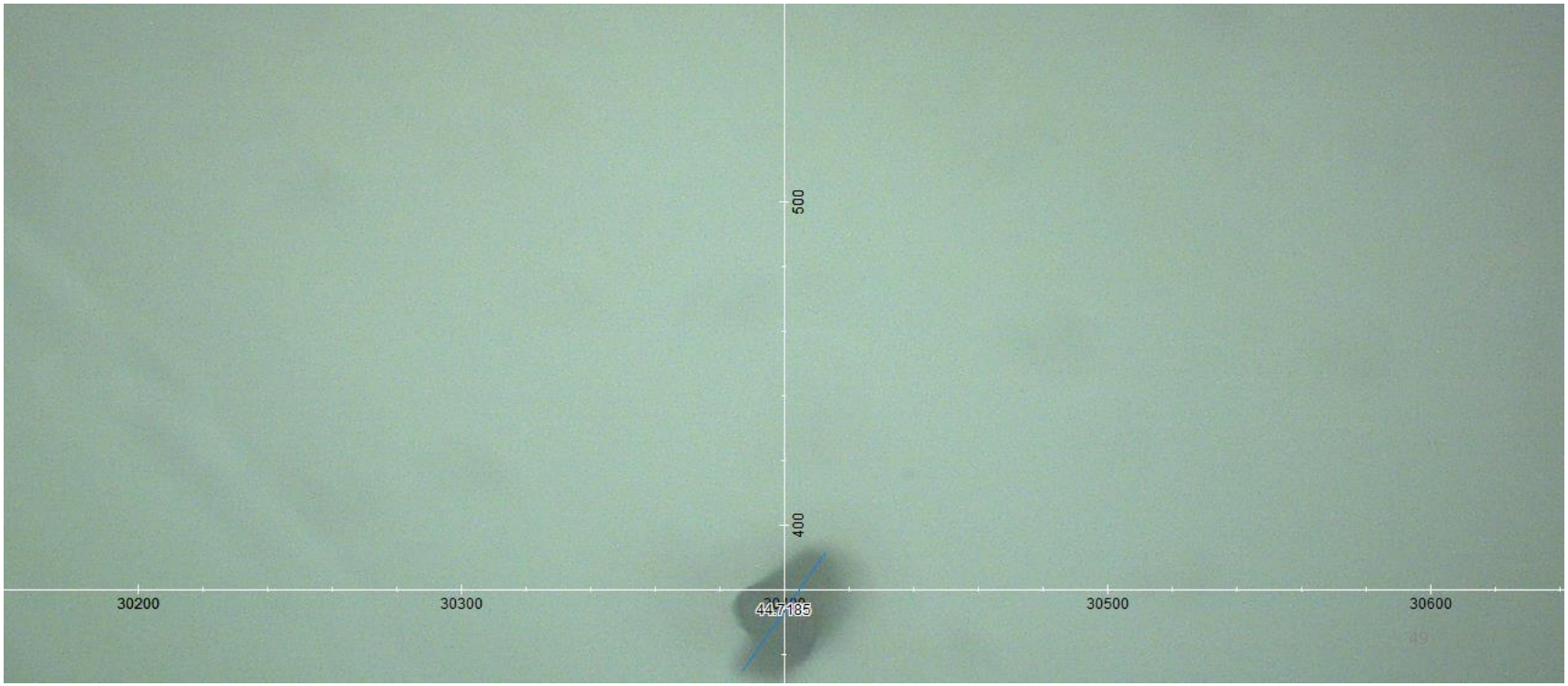

25. ASTRAZENECA
AZ MIT UP CARB6

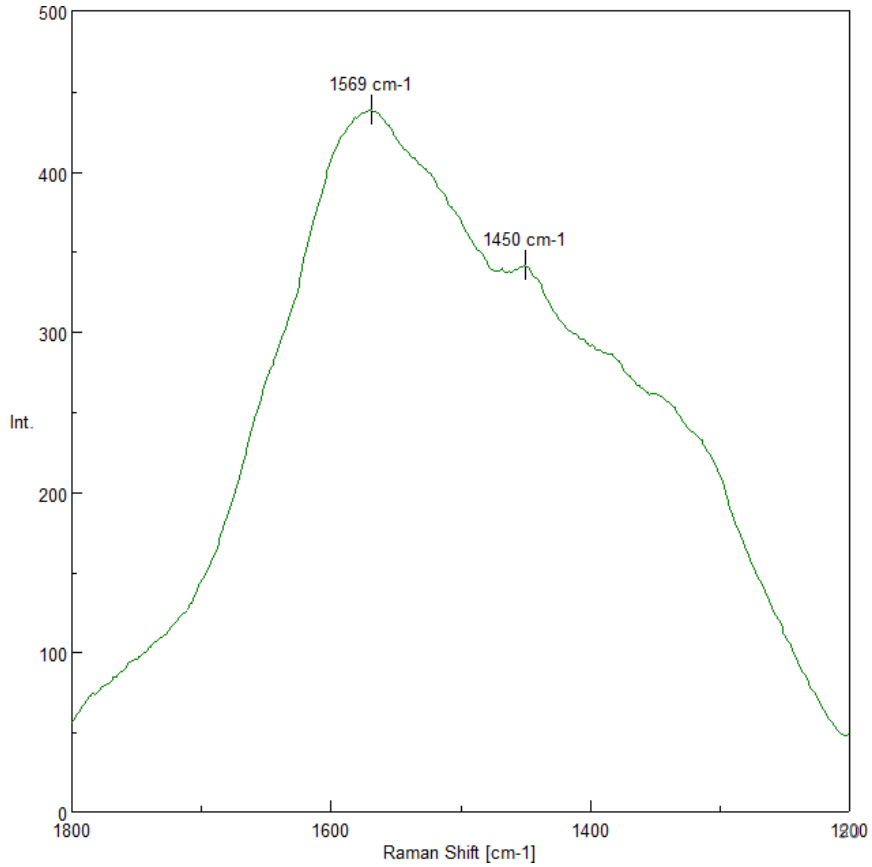

26. JANSSEN
JAN GO1

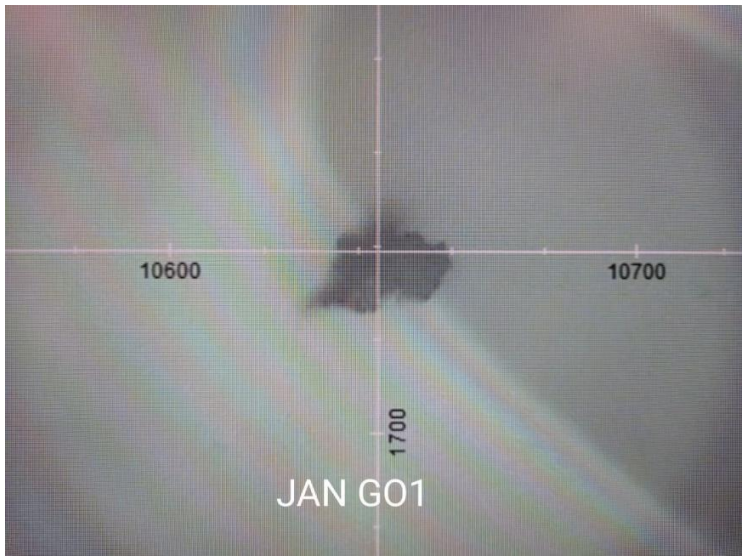

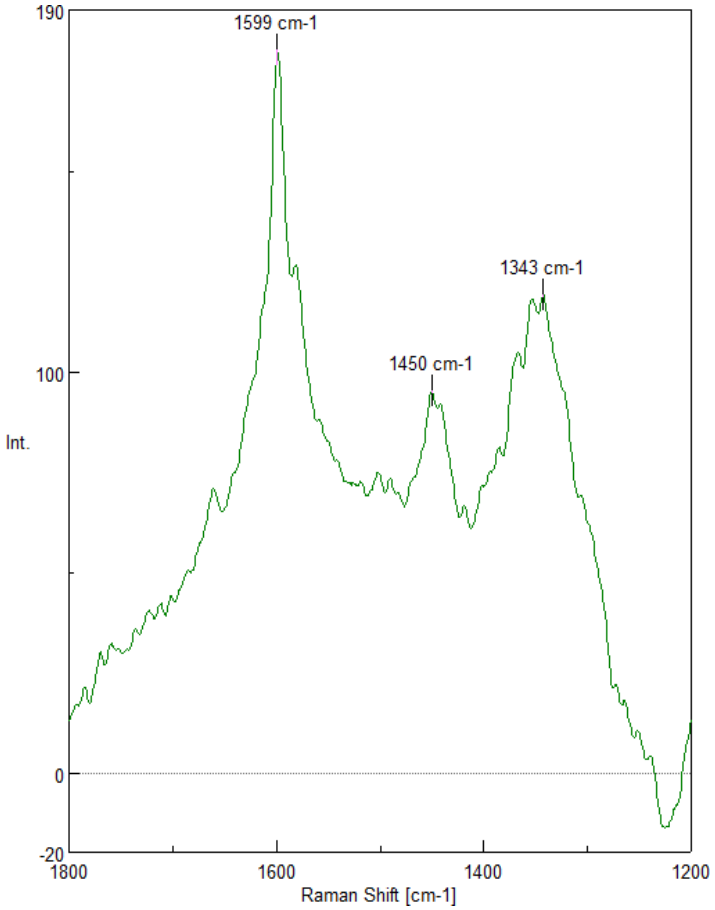

27. JANSSEN
JAN GO3

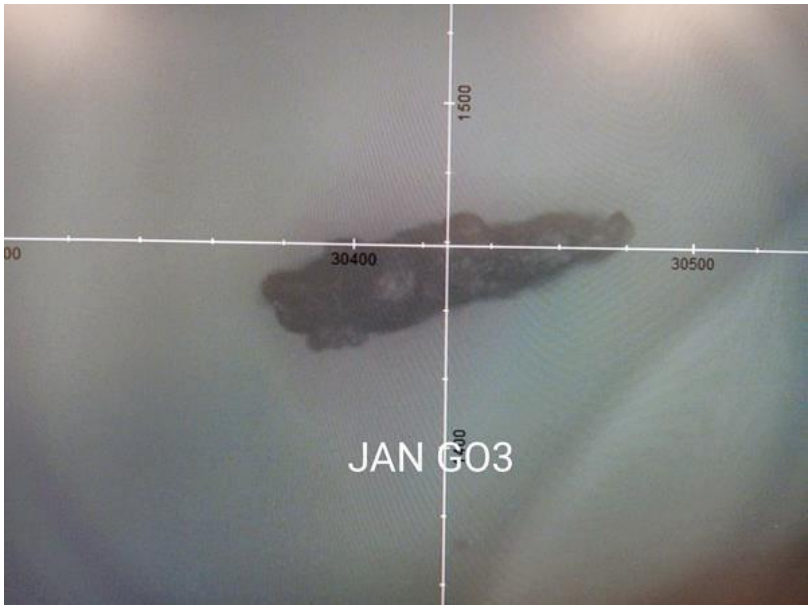

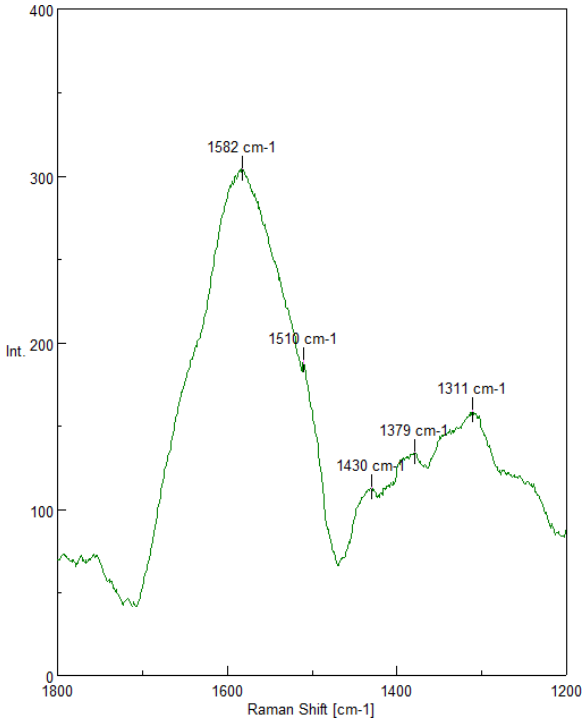

28. JANSSEN
JAN GO4